Determination of Dominant Failure Modes Using Combined Experimental and Statistical Methods and Selection of Best Method to Calculate Degradation Rates

by

Sanjay Shrestha

A Thesis Presented in Partial Fulfillment
of the Requirements for the Degree
Master of Science

Approved October 2014 by the
Graduate Supervisory Committee:

Govindasamy Tamizhmani, Chair
Bradley Rogers
Devrajan Srinivasan

ARIZONA STATE UNIVERSITY

December 2014

ABSTRACT

This is a two part thesis:

Part 1 of this thesis determines the most dominant failure modes of field aged photovoltaic (PV) modules using experimental data and statistical analysis, FMECA (Failure Mode, Effect, and Criticality Analysis). The failure and degradation modes of about 5900 crystalline-Si glass/polymer modules fielded for 6 to 16 years in three different photovoltaic (PV) power plants with different mounting systems under the hot-dry desert climate of Arizona are evaluated. A statistical reliability tool, FMECA that uses Risk Priority Number (RPN) is performed for each PV power plant to determine the dominant failure modes in the modules by means of ranking and prioritizing the modes. This study on PV power plants considers all the failure and degradation modes from both safety and performance perspectives, and thus, comes to the conclusion that solder bond fatigue/failure with/without gridline/metallization contact fatigue/failure is the most dominant failure mode for these module types in the hot-dry desert climate of Arizona.

Part 2 of this thesis determines the best method to compute degradation rates of PV modules. Three different PV systems were evaluated to compute degradation rates using four methods and they are: I-V measurement, metered kWh, performance ratio (PR) and performance index (PI). I-V method, being an ideal method for degradation rate computation, were compared to the results from other three methods. The median degradation rates computed from kWh method were within ±0.15% from I-V measured degradation rates (0.9-1.37 %/year of three models). Degradation rates from the PI method

were within ±0.05% from the I-V measured rates for two systems but the calculated degradation rate was remarkably different (±1%) from the I-V method for the third system. The degradation rate from the PR method was within ±0.16% from the I-V measured rate for only one system but were remarkably different (±1%) from the I-V measured rate for the other two systems. Thus, it was concluded that metered raw kWh method is the best practical method, after I-V method and PI method (if ground mounted POA insolation and other weather data are available) for degradation computation as this method was found to be fairly accurate, easy, inexpensive, fast and convenient.

DEDICATION

This thesis work at ASU-PRL is dedicated to my parents and my family, especially my sister Jesmina Shrestha for her constant motivation, love and support during my Master's program.

ACKNOWLEDGMENTS

First of all, I would like to thank my advisor/chair, Dr. Govindasamy Tamizhmani for his constant guidance, effort and supervision throughout my Master's thesis work. It was a great pleasure and honor to work with such a figurehead. I would also like thank my committee members Dr. Rogers and Dr. Srinivasan for their support during my work.

I really appreciated the opportunity to work at Arizona State University Photovoltaic Reliability Laboratory and for this I would like to thank Mr. Joseph Kuitche. His instructions and lessons were a great boost and help towards my work at PRL.

I was really grateful to work with some wonderful and hard-working individuals in the lab. My special thanks goes to Mohammad Naeem, Sai Tatapudi, Jaya Mallineni, Karan Rao Yeddidi, Brett Knisely, Bulent Bicer, Sravanthi Bopanna, Mathew Chica, Vidyashree Rajshekhar, Christopher Raupp and Neelesh Umachandran.

The funding and technical support of Salt River Project (SRP) is gratefully acknowledged. This work was partly funded by the DOE/SERIIUS project. And also, I would like to thank Bill Kazeta, Dan Wilson and Nicolas Quinones for their support and cooperation.

TABLE OF CONTENTS

Page

LIST OF TABELS……viii

LIST OF FIGURES……...x

CHAPTER

PART 1: DETERMINATION OF DOMINANT FAILURE MODES USING FMECA ON THE FIELD DEPLOYED C-SI MODULES UNDER HOT-DRY DESERT CLIMATE....1

1.1 INTRODUCTION 2

1.1.1 Background 2

1.1.2 Statement of the Problem 3

1.1.3 Objective 4

1.2 LITERATURE REVIEW 5

1.2.1 Durability and Reliability Definitions of PV Modules 5

1.2.2 Failure Modes and Degradation Modes 5

1.2.3 FMEA/FMECA 7

1.2.4 Risk Priority Number (RPN) 8

1.3 METHODOLOGY 13

1.3.1 Determination of Severity 14

CHAPTER Page

1.3.2 Determination of Detection 16

1.3.3 Determination of Occurrence 18

1.4 RESULTS AND DISCUSSIONS 20

1.4.1 Site 1: Frameless Modules (Model G) - One Axis Tracker 21

1.4.2 Site 2: Frameless Modules (Model BRO) - Ground Fixed Tilt 24

1.4.3 Site 3: Framed Modules (Model HP) - Rooftop Fixed Tilt 28

1.5 CONCLUSION 32

PART 2: DETERMINATION OF BEST METHOD TO CALCULATE DEGRADATION RATES 33

2.1 INTRODUCTION 34

2.1.1 Background 34

2.1.2 Statement of the Problem 35

2.1.3 Objective 35

2.2 LITERATURE REVIEW 36

2.2.1 PV Array Performance Modelling 36

2.2.2 Thermal Models 36

2.2.3 Sandia’s Thermal Model 37

2.2.4 SolarAnywhere Irradiance Models 39

2.2.5 POA Irradiance Model 41

CHAPTER Page

2.2.6 Perez Sky Diffuse Model 43

2.2.7 Performance Ratio (PR) 45

2.2.8 Performance Index (PI) 46

2.3 METHODOLOGY 48

2.3.1 Module IV Method in the Field 48

2.3.2 Metered Raw KWh Method 49

2.3.3 Performance Ratio (PR) Method....52

2.3.4 Performance Index (PI) Method....56

2.4 RESULTS AND DISCUSSION 59

2.4.1 Fielded Module IV Data Analysis....59

2.4.2 Metered Raw Energy (KWh) Data Analysis 61

2.4.3 Performance Ratio (PR) Data Analysis 69

2.4.4 Performance Index (PI) Data Analysis 72

2.4.5 Application of Performance Index 79

2.5 CONCLUSION....82

REFERENCES 84

LIST OF TABELS

Table Page

1 Key Failure Modes, Causes and Effects of PV Modules in Hot-Dry Climates 6

2 Determination of Parameter “S” (IEC 60812 Std.) 9

3 Determination of Parameter “O” (IEC 60812 Std.) 10

4 Failure Mode Detection Evaluation Criteria (IEC 60812 Std.) 11

5 Determination of Severity (S) 16

6 Determination of Detection (D) 18

7 Failure Mode Occurrence Related to Frequency and Probability of Occurrence (IEC 60812:2006 Std.) 19

8 Nameplate Specification of the Glass/Polymer Modules 20

9 Occurrence Ranking of Failure Modes of 2352 Modules of Site 1 (Model G) 21

10 Computation of Risk Priority Number (RPN) of Site 1 (Model G) 23

11 Occurrence Raking of Failure and Degradation Modes of 3024 Modules of Site 2 (Model BRO) 25

12 Computation of Risk Priority Number (RPN) of Site 2 (Model BRO) 26

13Occurrence Ranking of Failure Modes of 504 Modules of Site 3 (Model HP) 28

14 Computation of Risk Priority Number (RPN) of Site 3 (Model HP) 30

15 Empirically Determined Coefficients to Predict Module Back Surface Temperature [25] 39

16 Perez Model Coefficient for Irradiance [28] 44

17 Sky Clearness Bins [28] 45

Table Page

18 PV Systems Information..48

LIST OF FIGURES

Figure Page

1 Metric Definitions for Safety Failure, Reliability Failure, and Durability Loss 5

2 Backsheet Burn Due to Solder Bond Failure [1] 24

3 Broken Module with Zero Power in Site 2 (Reason for the Breakage Unknown) 27

4 IR Image of a Delaminated Cell Creating a Severe Hotspot Causing a Bubble in the Backsheet 30

5 RPN vs. Failure Mode of All Three Models Fielded in a Hot-Dry Climate of Arizona ...31

6 Satellite Image for Irradiance Estimation [26].....40

7 Satellite Based Modelled GHI vs. Measured GHI in Albuquerque, 1999 [27] 41

8 Flowchart of Degradation Rate Calculation from IV Measurement 49

9 Calculation of Degradation Rate per Year Using Just KWh Data i.e. Without Insolation and Temperature Data.....51

10 Fluctuation in Monthly Insolation from Average Insolation (1991-2010 NREL-NSRDB [30]) 52

11 Source of Insolation Data (Solar Anywhere Data) 53

12 Calculation of Degradation Rate per Year Using Performance Ratio (PR) i.e. with Irradiance.....55

13 Degradation Rate per Year Using Performance Index (PI) i.e. with the Adjustments 58

14 Histogram of Model G Degradation per Year Using Performance Measurement (IV) [1] 60

15 Histogram of Model CT Degradation per Year Using Performance Measurement (IV) 60

Figure Page

16 Histogram of Model HP Degradation per Year Using Performance Measurement (IV) 61

17 Degradation Rate Computation for Month of April for Model G 62

18 Histogram of Model G Raw KWh Degradation Rate per Year 62

19 Histogram of Model CT Raw KWh Degradation per Year.....63

20 Histogram of Model G Raw KWh Degradation per Year.....63

21 Monthly Deviation of Insolation in Phoenix from SolarAnywhere Data (1998-2013)...64

22 Histogram of Model G Degradation per Year Using KWh of 7 Months.....65

23 Histogram of Model CT Degradation per Year Using KWh of 7 Months 65

24 Histogram of Model HP Degradation per Year Using KWh of 7 Months 66

25 Monthly Variation of Insolation in San Diego, CA.....67

26 Monthly Variation of Insolation in Golden, CO.....68

27 Monthly Variation of Insolation in Newark, NJ 68

28 Monthly Variation of Insolation in Phoenix, AZ.....69

29 Degradation Rate per Year on Feb 1 of Model G Using PR Analysis.....70

30 Histogram of Model G Degradation per Year Using Performance Ratio (PR) 70

31 Histogram of Model CT Degradation per Year Using Performance Ratio (PR).....71

32 Histogram of Model HP Degradation per Year Using Performance Ratio (PR).....71

33 Degradation Rate per Year on Mar 1 of Model G Using PI Analysis 73

34 Histogram of Model G Degradation per Year Using Performance Index (PI) 73

35 Histogram of Model CT Degradation per Year Using Performance Index (PI).....74

36 Histogram of Model HP Degradation per Year Using Performance Index (PI).....74

37 Plot of Mean Degradation Rate per Year of Three Models Using Different Methods....75

Figure Page

38 Plot of Median Degradation Rate per Year of Three Models Using Different Methods 76

39 Deviation of Computed Degradation Rates from I-V Measured Rate 77

40 Monthly % Temperature Loss and Measured Output Energy for Model G In 2003.....80

41 Average Performance and Losses of Model G from 2003-2007.....80

42 Soiling Rate of Model CT from September to December 2006.....81

PART 1: DETERMINATION OF DOMINANT FAILURE MODES USING FMECA ON THE FIELD DEPLOYED c-Si MODULES UNDER HOT-DRY DESERT CLIMATE

1.1 INTRODUCTION

1.1.1 Background

Photovoltaic (PV) modules in the field can experience different types of failure modes and mechanisms, depending on the climatic condition, design, manufacturing control, installation type, and electrical configuration. Arizona State University's Photovoltaic Reliability Laboratory (ASU-PRL) has recently evaluated about 5900 (glass/backsheet) modules of three power plants in the hot-dry desert climate of Arizona to determine the dominant failure and degradation modes for this climate. The power plants are located in three sites (Glendale, Mesa, and Scottsdale) around Phoenix, Arizona, and have different module constructions and mounting structures: Site 1 – frameless glass/polymer modules (Model G), one-axis tracker mounting; Site 2 – frameless glass/polymer modules (Model BRO), ground fixed horizontal mounting; and Site 3 – framed glass/polymer modules (Model HP), roof top fixed tilt (10^{o}) mounting. All of the modules were visually inspected with the help of several non-destructive tools, such as IR camera, IV curve tracer, diode tester, etc., to detect the occurrence and effect of the degradation/failure modes experienced by the modules in the field. The reliability and durability issues of these PV modules are analyzed and reported elsewhere [1, 2].

This work carries out a statistical analysis on the results obtained from the previous two studies [1, 2] by using the Failure Mode, Effect, and Criticality Analysis (FMECA) technique. This technique has long been used in the automotive and electronic industries, and is introduced in this study for the PV industry. This method basically uses the Risk

Priority Number (RPN) for ranking failure modes, with the highest RPN being the worst failure mode. The approach taken in this study is site specific and considers all the performance and safety aspects within the particular power plant. The result of this study is useful not only for power plant developers, but also for the manufacturers. By knowing the dominant failure modes for particular climatic conditions, PV plant developers can choose the module designs that are resilient to those failure modes specific to their climatic condition. From the manufacturers' perspectives, the dominant mode will explain the manufacturing or design flaws. As a result, it will allow manufacturers to design a more reliable product for low warranty returns and claims.

1.1.2 Statement of the Problem

PV modules in the field degrade due to various environmental stresses and many other reasons. To design a better and reliable product, it is very important to know the failure mechanisms, modes and their causes, so that the product may be able to withstand these stresses for a long time. Since we know that, there are many field failure modes of PV modules and designing a new module which can endure all of the failure modes is somewhat impossible. Manufacturing a new reliable product is a step-by-step enhancement in product design and thus, it is very crucial to know the dominant failure modes which impact the performance, reliability and safety of the module or system. So now the question arises, how do we know which are the most dominant failure modes? Basically, this thesis work explains the statistical reliability tool, FMECA and uses it to determine the most dominant failure modes of c-Si modules under hot and dry climatic condition of Arizona.

1.1.3 Objective

The main objectives of the study are as follows:

- Determine all the possible failure modes in the field from field inspection as well as from literature.
- Determine the severity, occurrence and detectability of these failure modes.
- Rank the failure modes according to their impact on performance and safety to the system or property.
- Determine the most dominant failure modes under hot and dry climate.

1.2 LITERATURE REVIEW

1.2.1 Durability and Reliability Definitions of PV Modules

Durability loss can be described as a soft loss leading to the degradation of the modules meeting the warranty limit [3]. Reliability failure can be described as a hard failure leading to the degradation of the module beyond the warranty limit. Figure 1 shows the metric definitions for safety failure, reliability failure, and durability loss.

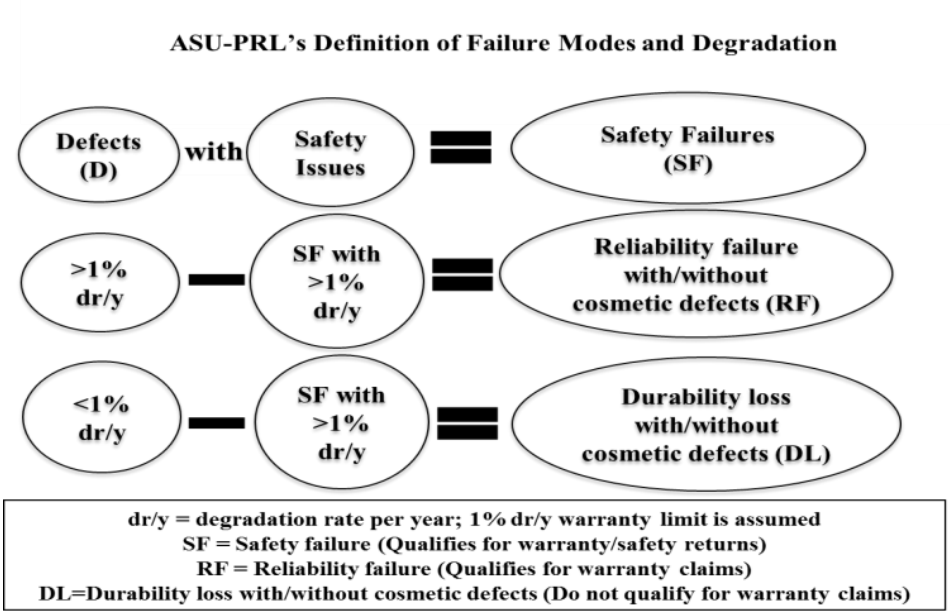

1 Metric Definitions for Safety Failure, Reliability Failure, and Durability Loss

1.2.2 Failure Modes and Degradation Modes

The failure and degradation modes of PV modules are dictated by the design/packaging/ construction and/or the field environment in which the modules operate. Failure modes can be triggered from different causes and can have different effects on PV modules [3]. Table

1 shows the overview of a few key failure modes, their causes and effects in hot-dry climatic conditions [1-3, 4-12].

1 Key Failure Modes, Causes and Effects of PV Modules in Hot-Dry Climates

Failure Cause	**Failure Mode**	**Effects**
UV light; humidity; contamination from the material; tempering process caused by stress and weakened adhesion	Encapsulant delamination	Power degradation; optical decoupling of materials; reverse-bias heating; transmission loss
High temperature thermal stress UV Light Hot solder joints	Discoloration/ browning	Power degradation; transmission loss
Movement of cells and cell interconnect; encapsulant gassing due to overheating; poor adherence of cell metallization; expansion & contraction of entrapped moisture & air; unframed laminates	Backsheet delamination/ peeling off	Safety hazards on rainy days; power degradation; corrosion (moisture and other contaminant penetration)
Coarsening; thermo mechanical fatigue; improper design and soldering process; less number of solder bonds	Solder bond fatigue/ failure	Power degradation; backsheet burn; High series resistance; hotspots
Shading; faulty cell or group of cells; bypass diode failure; solder bond failure	Hotspots	Overheat; backsheet/ encapsulant burn; power degradation
Moisture/Humidity ingress; inappropriate encapsulant;	Metallization discoloration	Open circuit failure; delamination; high series resistance; hotspots
Restricted heat dissipation; thermal runaway due to moving shadow	Bypass diode failure	Hotspot; fire hazard; junction box damage

1.2.3 FMEA/FMECA

Failure Modes and Effects Analysis (FMEA) is a qualitative method of reliability analysis (failure analysis) of any system or component or item. This is a systematic procedure that analyzes a system or a component of all possible failure modes, their cause and effect on performance as well as on other elements in a system. This analysis is mainly done in Reliability, Safety and Quality Engineering, which basically involves reviewing as many components, assemblies, and subsystems to identify failure modes, their causes and effects. During the design phase, the result of this analysis prioritizes the failures according to their consequences, occurrence, and detectability, thus drawing attention to eventual weaknesses in the system, in such a way as to reduce failures with necessary modifications and, more generally, improve reliability [13, 14].

FMECA extends FMEA with an addition of detailed quantitative analysis of criticality of failure modes. FMECA is essentially a method to identify the potential failure modes of a product or a process or a device or a system manufactured with different technologies (electrical, mechanical, hydraulic, etc.) or the combination of such technologies. Ideally, FMECA is conducted in the product design or process development stage, or after a quality function deployment to a product, but conducting it on fielded systems/products also yields benefits. FMEA/FMECA analysis allows a good understanding of the behavior of a component of a system, as it determines the effect of each failure mode and its causes. This assigns a rank to each of the failure modes according to their criticality, occurrence, and detectability. The study of criticality quantifies the effect of each failure mode, so that the effect of these failures could be minimized prior to action [14].

In the FMEA/FMECA analysis, the following procedures are taken into account [14]:

- System Description: Defines the system, including its functional, operative, and environmental requirements.
- Definition of Failure Modes: The modes, the causes and the effects of failures, their relative importance and, in particular, their means of propagation are defined. The presence of failure mode indicates that there is a failure in the system, the manner in which an item fails.
- Identifying the causes of failures: The causes of each failure mode are identified.
- Identifying the effects of failure modes: The effects of each failure mode in the system leading to different degradation or harm to environment or to the system are identified.
- Definition of measures and methods for identifying and isolating failures: Defines the ways and methods for identifying and isolating failures.
- Classification of the severity of final effects: The classification of the effects is carried out according to the nature of the system under examination, the performance and functional characteristics of the system, especially in regard to operator safety, and finally, guarantee requirements.

1.2.4 Risk Priority Number (RPN)

This follows the IEC 60812 2006-01 Standard [15]. The RPN is one of the approaches for quantification of the criticality of the failure mode. A measurement of RPN is therefore:

RPN = S * O * D

Where:

"S" means severity, which is an estimate of how strongly the effects of the failure will affect the system or the user. This is the measure of severity or criticality of the failure mode and is a non-dimensional number. Table 2 shows the criteria for determining severity according to the IEC 60812 widely used in the automotive industry.

2 Determination of Parameter "S" (IEC 60812 Std.)

Severity	Criteria	Ranking
None	No discernible effect	1
Very minor	Fit & finish/squeak and rattle item do not conform. Defect noticed by discriminating customers (less than 25%)	2
Minor	Fit & finish/squeak and rattle item do not conform. Defect noticed by discriminating customers (less than 50%)	3
Very low	Fit & finish/squeak and rattle item do not conform. Defect noticed by discriminating customers (less than 75%)	4
Low	Item operable but comfort/convenience item(s) operable at a reduced level of performance. Customer somewhat dissatisfied.	5
Moderate	Item operable but comfort/convenience item(s) inoperable. Customer dissatisfied.	6
High	Item operable but at a reduced level of performance. Customer very dissatisfied.	7
Very High	Item inoperable (loss of primary function)	8
Hazardous with warning	Very high severity ranking when a potential failure mode affects safe operation and/or involves non-compliance with government regulation with warning.	9
Hazardous without warning	Very high severity ranking when a potential failure mode affects safe operation and/or involves non-compliance with government regulation without warning	10

“O” means occurrence, which denotes the probability of occurrence of a failure mode for a predetermined or stated time period. It may be defined as a ranking number rather than the actual probability of occurrence. Table 3 shows the occurrence ranking related to frequency.

3 Determination of Parameter “O” (IEC 60812 Std.)

Occurrence	Frequency	Ranking
Remote: Failure is unlikely	<= 0.01 per thousand items	1
Low: Relatively few failures	0.1 per thousand items	2
	0.5 per thousand items	3
Moderate: Occasional failures	1 per thousand items	4
	2 per thousand items	5
	5 per thousand items	6
High: Repeated failures	10 per thousand items	7
	20 per thousand items	8
Very high: Failure is almost inevitable	50 per thousand items	9
	>= 100 per thousand items	10

“D” means detection, which is an approximation of the chance to identify and eliminate the failure before the system or user is affected. This number is usually ranked in reverse order from the severity or occurrence numbers: the higher the detection number, the less probable

the detection is. This means that the low probability of detection will yield to higher RPN. Table 4 shows the detection ranking used in IEC 60812.

4 Failure Mode Detection Evaluation Criteria (IEC 60812 Std.)

Detection	Criteria: Likelihood of Detection by Design Control	Ranking
Almost certain	Design Control will almost certainly detect a potential cause/mechanism and subsequent failure mode	1
Very high	Very high chance the Design Control will detect a potential cause/mechanism and subsequent failure mode	2
High	High chance the Design Control will detect a potential cause/mechanism and subsequent failure mode	3
Moderately high	Moderately high chance the Design Control will detect a potential cause/mechanism and subsequent failure mode	4
Moderate	Moderate chance the Design Control will detect a potential cause/mechanism and subsequent failure mode	5
Low	Low chance the Design Control will detect a potential cause/mechanism and subsequent failure mode	6
Very low	Very low chance the Design Control will detect a potential cause/mechanism and subsequent failure mode	7
Remote	Remote chance the Design Control will detect a potential cause/mechanism and subsequent failure mode	8
Very remote	Very remote chance the Design Control will detect a potential cause/mechanism and subsequent failure mode	9
Absolutely uncertain	Design Control will not and/or cannot detect a potential cause/mechanism and subsequent failure mode; or there is no Design Control	10

The computed RPN, together with the level of severity, determines the worst/critical failure mode, so that the focus could be concentrated to mitigate the effects from the failure. This means that if there are failure modes with similar or identical RPN, the failure modes that

are to be addressed first are those with the higher severity numbers. The failure modes are then ranked according to their RPN, and high priority is assigned to high RPN.

As we know from the above, the RPN is the product of S, O, and D, and the evaluation of RPN can present some problems such as [14, 16]:

- Gaps in the range: The RPN values are not continuous, but have only 120 unique values: 88% of the range is empty. Thus, the numbers 11, 22, 33,.., 990 which are all multiples of 11 cannot be formed and are excluded. Similarly, all multiples of 13, 17, 19, etc., are excluded. The largest number is 1000, but 900 is the second largest followed by 810, 800, 729, and 720.
- Duplicate RPNs: Different values of the parameters may generate identical RPN values. The RPN numbers 60, 72, and 120 can each be formed from 24 different combinations of S, O, and D. Similarly, seven RPN numbers, 24, 36, 40, 48, 80, 90, and 180, can be formed from 21 different combinations.
- High sensitivity to small changes: Multiplying the numbers comprising the RPN is intended to magnify the effects of high risk factors. Thus, even a small variation in one of the parameters implies a notable variation in the RPN value.
- Inadequate scale of RPN: The difference in RPN value might appear negligible, whereas it is in fact significant. For example, the RPN_1 with 3, 4, and 5 as S, O, and D, respectively, gives the value of 60, whereas the RPN_2 with 3, 5, and 5 gives 75. In fact, in RPN_2 the failure mode has the twice the occurrence, but the RPN value is not doubled. This explains that the RPN values cannot be compared linearly [14, 16].

1.3 METHODOLOGY

All the modules were inspected using a systematic visual inspection, IR camera, IV Tracer, and a diode tester. The performance parameters of all the strings and of all the modules in the best, worst, and median strings were obtained. The failure modes of these modules were identified using the above evaluation methods, and then the potential causes and effects of these modes were determined. The approach used in this study is very site specific, so the location and the construction of the site are also taken into account for failure mode effects.

The failure modes were identified visually or by the use of some tools mentioned earlier, but the cell/metal and metal/metal interface degradations/failures including solder bond fatigue/failures were derived from the series resistance (Rs) estimations. Due to the cyclic loading, such as thermal, mechanical or electrical repetitive stress, deteriorations in the interfaces including solder bond fatigue/failure may be induced [4]. In the hot-dry climatic conditions investigated in this study, thermal cyclic loading is considered as a major or the primary stress due to the difference in the thermal coefficients of expansion between the materials including silicon wafer and metallization, metallization and solder, and metal ribbon and solder. For c-Si cells, Meier et al. [17] have shown that the series resistance is arising from seven components: front busbar, front gridlines, contact interface (between grid lines and emitter), emitter sheet, silicon substrate, back metal and back busbar. For c-Si modules, the series resistance is arising from four additional components: busbar/ribbon interface solder bonds (cell interconnect solder bonds), ribbon/ribbon interface solder bonds (string interconnect solder bonds), cell interconnect copper ribbons and string

interconnect copper ribbons. Thermal cyclic loading over the fielded years is expected stress on these cell and module level interfaces (contact interface of cell, cell interconnect solder bonds and string interconnect solder bonds) leading to increase in the series resistance. To determine which of three interfaces is dominating, a deconstructive analysis (both materials and four probe electrical resistance) needs to be carried out which is a subject of future investigation of this research group. The Rs of each module was estimated from the performance data using the empirical expression from Dobos [18] as shown as in Equation 1:

$$\mathrm{Rs} = \mathrm{CS} * \frac{\mathrm{Voc}-\mathrm{Vmp}}{\mathrm{Imp}} \qquad (1)$$

Where CS = 0.32 for mono c-Si module and 0.34 for poly c-Si module

1.3.1 Determination of Severity

The severity of the failure mode is determined in consideration of the effect on the performance and safety raised by that failure mode to the specific site, but the highest rank in the severity table is given to the safety issue as it is a threat/hazard to the personnel or to the property. In this analysis, the severity numbers from 8 to 10 are related to safety issues, whereas the numbers from 7 to 1 depend on the performance factor. The severity ranking of the failure mode is done with respect to the degradation rate per year of the module that is having that particular failure mode as a dominant mode in inducing the degradation. The degradation is assumed to be linear and it is computed using Pmax drop as shown as in Equation 2 below:

$$\text{Degradation rate per year(Rd)} = \frac{(\text{Pmax drop} * 100)}{(\text{Rated Pmax} * \text{age of operation})} \quad (2)$$

Where,

Pmax drop = Rated Pmax- Measured present day Pmax

The degradation rate of less than 0.3% per year has been reported in some field deployed modules. Thus, the least severity criteria are given as “No effect” and “Insignificant” to the failure modes contributing to Rd (degradation rate per year) less than 0.3% or approximately to 0.3%. Based on a review of more than 2000 reported data, Jordan and Kurtz showed median and mean degradation of 0.5% and 0.8% per year, respectively, for several diversified climatic conditions [19]; hence, a severity rank from 3 to 5 is given to the failure mode contributing to 0.5% to 0.8% Rd. Table 5 shows the ranking criteria for the parameter S (Severity).

5 Determination of Severity (S)

Ranking	Severity Criteria	Severity
1	No effect, Rd < 0.3%	None
2	Insignificant, Rd approx. to 0.3%	Very minor
3	Minor Cosmetic defect, Rd < 0.5%	Minor
4	Cosmetic defect with Rd < 0.6%	Very low
5	Reduced performance, Rd < 0.8%	Low
6	Performance loss approx. to typical warranty limit, Rd approx. to 1%	Moderate
7	Significant degradation, Rd approx. to 1.5%	High
8	Remote safety concerns, Rd < 1%	Hazardous with operable performance
9	Remote safety concerns, Rd < 2%	Hazardous with reduced level performance
10	Safety hazard, Catastrophic	Catastrophic

1.3.2 Determination of Detection

Kuitche [20] et al. used an accelerated testing and qualification testing technique to determine the likelihood (probability) of detection of a failure mode. However, this system FMECA analysis follows the field evaluation approach for the detectability of failure modes. The likelihood of detection of a failure mode is determined from the field employed modules in the power plant during inspection. The detection number 1 is given if the monitor system, i.e., field control mechanism detects the failure mode in the scheduled/

regular maintenance or event-triggered inspections or inverter shut down in case of arc fault. Basically, the ranking goes higher as different measures are taken to detect the failure mode. If the failure mode is detected visually, the number 2-3 is given. If the failure mode is detected using a conventional tool such as IR camera, megger test, etc., the ranking 4-5 is given depending upon the likelihood. The ranking of 6-7 is given if the failure mode is detected using non-conventional handheld tools such as diode/line checker. If the failure mode is detected using performance measurement equipment like IV tracer, then a ranking of 8-9 is given depending upon their likelihood. Finally, if the failure mode is detectable using advanced equipment only such as EL Imaging, UV fluorescence, module QE, and so on, which can be done only in the lab, then the highest number 10 is given. Table 6 shows the detailed detection ranking table used in this study.

6 Determination of Detection (D)

Ranking	Criteria: Likelihood	Detection
1	Monitoring System itself will detect the failure mode with warning 100%	Almost certain
2	Very high probability (most likely) of detection through visual inspection	Very high
3	50/50 probability (less likely) of detection through visual inspection	High
4	Very high probability (most likely) of detection using conventional handheld tool e.g. IR, Megger	Moderately high
5	50/50 probability (less likely) of detection using conventional handheld tool e.g. IR, Megger	Moderate
6	Very high probability (most likely) of detection using non-conventional handheld tool e.g. diode/line checker	Low
7	50/50 probability (less likely) of detection using non-conventional handheld tool e.g. diode/line checker	Very low
8	Very high probability (most likely) of detection using performance measurement equipment e.g. IV tracer	Extremely Low
9	50/50 probability (less likely) of detection using performance measurement equipment e.g. IV tracer	Remote
10	Detection impossible in the field	Absolutely uncertain

1.3.3 Determination of Occurrence

The occurrence ranking is performed to the real field data considering the time period of the field exposure of the module. Table 7 shows the ranking of occurrence according to the computed frequency of each failure mode. The cumulative number of module failures per thousand per year (CNF) is computed as shown as in Equation 3.

$$\frac{CNF}{1000} = \sum system\ (\%\ defects) * \frac{10}{\sum system\ (operating\ time)} \qquad (3)$$

7 Failure Mode Occurrence Related to Frequency and Probability of Occurrence (IEC 60812:2006 Std.)

Failure Mode Occurrence	Frequency CNF/1000	Ranking O
Remote: Failure is unlikely	<= 0.01 module per thousand per year	1
Low: Relatively few failures	0.1 module per thousand per year	2
	0.5 module per thousand per year	3
Moderate: Occasional failures	1 module per thousand per year	4
	2 module per thousand per year	5
	5 module per thousand per year	6
High: Repeated failures	10 module per thousand per year	7
	20 module per thousand per year	8
Very high: Failure is almost inevitable	50 module per thousand per year	9
	>= 100 module per thousand per year	10

1.4 RESULTS AND DISCUSSIONS

This chapter explains the implementation of the FMECA technique to the real field data and the results extracted from the analysis. In this analysis, three different sites with different orientation under hot and dry climate of Arizona were chosen. From the inspection of these three sites, two sets of data were collected: count data of the failure modes for the occurrence ranking and performance data of the modules to determine severity ranking. The FMECA technique used in this study was specific to each site, therefore, the technique was applied individually to each site. Table 8 shows the nameplate specification of three glass/polymer models from three different sites used in this analysis. Following paragraphs give the detailed results from each site.

8 Nameplate Specification of the Glass/Polymer Modules

Model	Nameplate Specifications					
	Isc (A)	Voc (V)	Im (A)	Vm (V)	FF (%)	Pm (W)
Model G	7.30	20.60	5.40	16.60	68.97	106.25
Model BRO	4.80	21.70	4.40	17.00	71.81	75.00
Model HP	3.83	68.70	3.59	55.80	76.13	200.00

1.4.1 Site 1: Frameless Modules (Model G) - One Axis Tracker

In this site, the Model G modules are mounted in one-axis north-south horizontal axis tracker. There were 2352 frameless glass/polymer monocrystalline-Si modules, and those had been fielded for 12 years at the time of inspection. The nameplate specification of this Model G can be seen in Table 7. From the count data, the frequency of the occurrence of failure modes is computed using the formula discussed in the previous section. Metallization discoloration was observed to be the most frequent degradation/failure mode, and the ranking of 8 was given. Table 9 shows the computed frequency and occurrence ranking of each failure mode for this site.

9 Occurrence Ranking of Failure Modes of 2352 Modules of Site 1 (Model G)

No	Failure/Degradation Mode	No. of Defects	Frequency CNF/1000	Ranking O
1	Encapsulant Delamination	217	7.69	7
2	Discoloration/ Browning	98	3.47	6
3	Backsheet Delamination/ Peeling off	12	0.43	3
4	Metallization discoloration	690	24.45	8
5	Solder bond with/without gridline contact fatigue/failure	89	3.15	6
6	Hotspots	45	1.59	5
7	Bypass diode failure	26	0.92	4

From the performance data, the degradation and performance of the modules were evaluated for the determination of the severity (S) of the failure modes. In these specific

modules (Model G), very minor encapsulant delamination, metallization discoloration, and encapsulant yellowing were observed, and they were only cosmetic defects with no significant degradation in Isc and in the performance of the module; so, the minor severity of 3 was given to these failure modes.

Solder bond fatigue/failure and hotspots were found to be the most severe defects. Two modules had zero power because of both ribbon-ribbons solder bond failure, and four modules had a ribbon-ribbon (string interconnect) solder bond failure contributing to a drop in Vmax, Voc, and Pmax as one of the string in the module was disconnected. From the visual inspection, it was seen that all the modules with solder bond failure and hotspot issue had backsheet burns. From the performance data, an approximately 20% increase in series resistance was found as a result of cell/metal and/or metal/metal interface issues including solder bond fatigue. A mean degradation rate of 2.83% per year was found for the 31 hotspot modules as compared with the mean degradation rate of 0.94% per year for the non-hotspot modules. Thus, the severity of 10 and 9 are given to these failure modes, respectively. Bypass diode failure and backsheet delamination are other safety issues and are given the severity of 8 due to their remote safety concern (due to remote shading in this specific site) and lesser influence in the performance drop in this site. In this site, all the failure/degradation modes were detected either by visual inspection or by using conventional and no-conventional tools such as diode checker, IR Camera, IV tracer and so on. The ranking of 2 was given to those failure modes which were detected visually, whereas hotspot was detected using IR image, so ranking of 4 was given. Solder bond failure and bypass diode failure were detected using diode/line checker, so a ranking of 6

was given to both of these failure modes. Table 9 shows the S, O, and, D ranking and computed RPN of each failure mode.

10 Computation of Risk Priority Number (RPN) of Site 1 (Model G)

No.	Failure/Degradation Modes	S	O	D	RPN
1	Encapsulant Delamination	3	7	2	42
2	Discoloration/Browning	3	6	2	36
3	Backsheet Delamination/Peeling off	8	3	2	48
4	Metallization discoloration	3	8	2	48
5	Solder bond with/without gridline contact fatigue/failure	10	6	6	360
6	Hotspot	9	5	4	180
7	Bypass diode failure	8	4	6	192

From Table 10, solder bond fatigue/failure can be seen as the dominant degradation/failure mode for this site, as it has the highest RPN of 360. Figure 2 shows the solder bond safety failure causing the burning of backsheet and interconnect breakage of a module in site 1. Minor cosmetic defects, such as metallization discoloration, encapsulant browning, and delamination, had the least RPN ranking as they are responsible for only slight, if any, drop in the performance, so, they can be ignored for this module type (Model G) for this hot-dry desert climatic site.

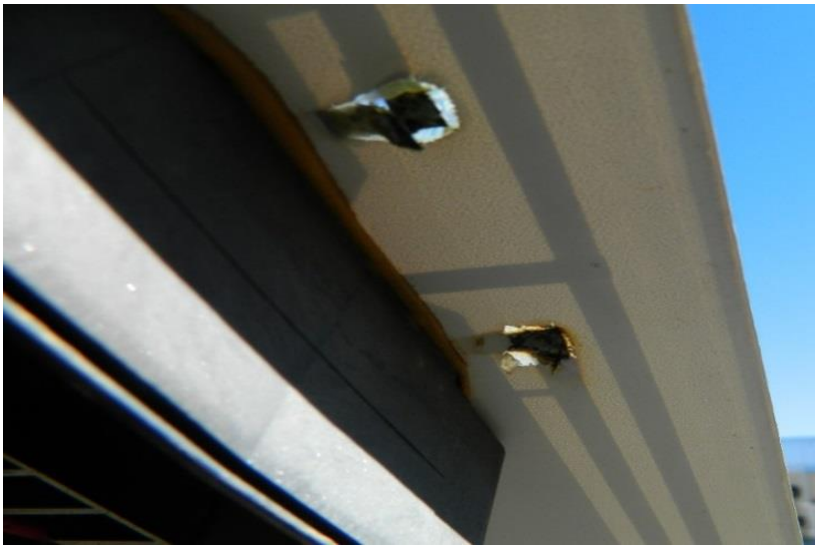

2 Backsheet Burn Due to Solder Bond Failure [1]

1.4.2 Site 2: Frameless Modules (Model BRO) - Ground Fixed Tilt

Site 2 is 16 years old and has 3024 frameless glass/polymer monocrystalline-Si modules (Model BRO) installed in a fixed horizontal position. From the inspection of the site, the encapsulant discoloration was found to be the most frequent defect/degradation mode, as all the modules were found to be browned. Seen from the increase of Rs in all the modules, the solder bond fatigue was given the ranking of 9. Table 11 shows the results of count data and occurrence ranking of the failure modes.

11 Occurrence Raking of Failure and Degradation Modes of 3024 Modules of Site 2 (Model BRO)

No	Failure Modes/ Defects	No. of defects	Frequency CNF/1000	Ranking O
1	Discoloration/Browning	3024	62.50	9
2	Backsheet Delamination/Warping	31	0.64	3
3	Solder bond with/without gridline contact fatigue/failure	3024	62.50	9
4	Hotspots	5	0.10	2
5	Glass breakage/damage	1	0.02	1
6	Bypass diode failure	2	0.04	2

From the performance data, the degradation rate per year was calculated for all the tested modules for the determination of the severity (S). For these specific modules (Model BRO), hotspots were found to be minor as they were only having 6-7^{o}C of temperature difference and did not raise any safety concern to the site/module, so only a minor severity of 2 was given. The worst module of the plant had a degradation of 1.7% per year and an increase of series resistance by 40%; therefore, the severity of 5 was given to this failure/degradation mode. In the same module, encapsulant browning contributed to approximately 1% degradation per year, so the severity of 6 was given to this mode. A severity of 8 was given to backsheet delamination, as it was a safety concern with less impact in performance, whereas glass breakage was a catastrophic failure so the highest severity of 10 was given to this mode. In these specific modules, the bypass diode failed in

open circuit mode in two modules, so the performance of the modules was not affected, but it raised a remote safety concern to the module in case of shading, so the severity of 8 was given. Table 11 shows the severity ranking of all the failure modes.

Failure modes such as discoloration, backsheet delamination, and glass breakage were detected visually, so the detection ranking of 2 was given. Solder bond fatigue, hotspot, and bypass diode failure were detected using IV tracer, IR camera, and diode checker, respectively, so the ranking of 8, 4, and 6 were given respectively according to the detection criteria table in the previous section. Table 11 below shows the S, O, and D ranking of all the failure modes and RPN computation of the site.

12 Computation of Risk Priority Number (RPN) of Site 2 (Model BRO)

No	Failure/Degradation Modes	S	O	D	RPN
1	Solder bond with/without gridline contact fatigue/failure	5	9	8	360
2	Discoloration/Browning	6	9	2	108
3	Backsheet Delamination/Peeling Off	8	3	2	48
4	Bypass diode failure	8	2	6	96
5	Hotspots	2	2	4	16
6	Glass Breakage/Damage	10	1	2	20

3 Broken Module with Zero Power in Site 2 (Reason for the Breakage Unknown)

From Table 12, solder bond fatigue with/without gridline interface deterioration and discoloration can be seen as the dominant degradation/failure modes for this site, as they have the highest RPN of 360 and 108, respectively. Solder bond fatigue contributed to an increase in series resistance, whereas discoloration was responsible for transmission loss. Nonetheless, these reliability failure modes were not a safety issue in this site; their high occurrence and influence to high performance loss, RPN values of these modes were elevated. The hotspot in this site was insignificant, with no effect in performance as well as in safety, which is being reflected from its RPN value; consequently, it can be ignored for this site. The other three failure modes were safety failures but because of their low frequency, their RPN values were ordinary. Figure 3 shows the only one broken module of this site; however, the reason for this breakage is unclear.

1.4.3 Site 3: Framed Modules (Model HP) - Rooftop Fixed Tilt

Site 3 is a rooftop system and has been installed for five years with 504 glass/polymer monocrystalline-Si modules (Model HP). The modules are installed at 10^{o} fixed tilt facing south. Table 13 shows the count data of all the failure modes and their respective occurrence frequency and ranking. Backsheet browning, encapsulant discoloration, and solder bond fatigue were seen in all the modules, and from the computation of the frequency of occurrence, a ranking of 10 was given to these failure modes. Ranking for other failure modes were about 3-4 because of their low count in the site.

13Occurrence Ranking of Failure Modes of 504 Modules of Site 3 (Model HP)

No	Failure Mode/Defects	No. of Defects	Frequency CNF/1000	Ranking O
1	Backsheet Browning	504	166.67	10
2	Backsheet Bubbling/Warping	2	0.66	3
3	Solder bond with/without gridline contact fatigue/failure	504	166.67	10
4	Hotspots	4	1.32	4
5	Encapsulant Delamination	2	0.66	3
6	Encapsulant Discoloration	504	166.67	10

From the performance data, the degradation rate per year was calculated for all the tested modules for the determination of the severity (S). Backsheet browning was seen in between the cells, so it was given insignificant severity. Slight encapsulant discoloration was seen above the junction box which was responsible for minor performance loss, so the severity ranking of 3 was given. From the performance data, the increase in series resistance was

found to be approximately 20%. Thus, degradation of approximately 0.7% per year in the worst module can be related to the increase in series resistance. Therefore, the severity of 5 was given to interface/solder bond fatigue.

Other failure modes were safety-related issues, so the ranking was given from 8 to 10. The severity of 8 was given to backsheet bubbling and hotspot, as they were safety concerns with less impact in performance, whereas encapsulant delamination was causing one module to have a hotspot and a power drop of 50% on another module. Moreover, both of these modules had backsheet bubbling, so the severity of 9 was given to encapsulant delamination. Table 14 shows the severity ranking of all the failure modes. Failure/degradation modes, such as encapsulant discoloration, backsheet bubbling, browning and encapsulant delamination, were detected visually so the detection ranking of 2 was given. Solder bond fatigue and hotspot were detected using IV tracer and IR camera, so the ranking of 8 and 4 were given respectively. Table 14 shows S, O, and D ranking of all the failure/degradation modes and RPN computation of the site 3.

From Table 14, the solder bond fatigue can be seen as the dominant degradation/failure modes for this site, as it has an RPN of 400. Encapsulant discoloration and backsheet browning can be ignored for this site as they were minor as can be seen from their low severity. Others were remote safety issues and they had low RPN because of their low frequency. Figure 4 shows an IR image of a partially delaminated cell causing a severe hotspot and eventually, to bubble the backsheet (substrate). Encapsulant delamination was severe in this site but its low occurrence was responsible for the low RPN.

14 Computation of Risk Priority Number (RPN) of Site 3 (Model HP)

No	Failure/Degradation Modes	S	O	D	RPN
1	Backsheet Browning	2	10	2	40
2	Backsheet Bubbling/Warping	8	3	2	48
3	Solder bond with/without gridline contact fatigue/failure	5	10	8	400
4	Hotspots	8	4	4	128
5	Encapsulant Delamination	9	3	2	54
6	Encapsulant Discoloration	3	10	2	60

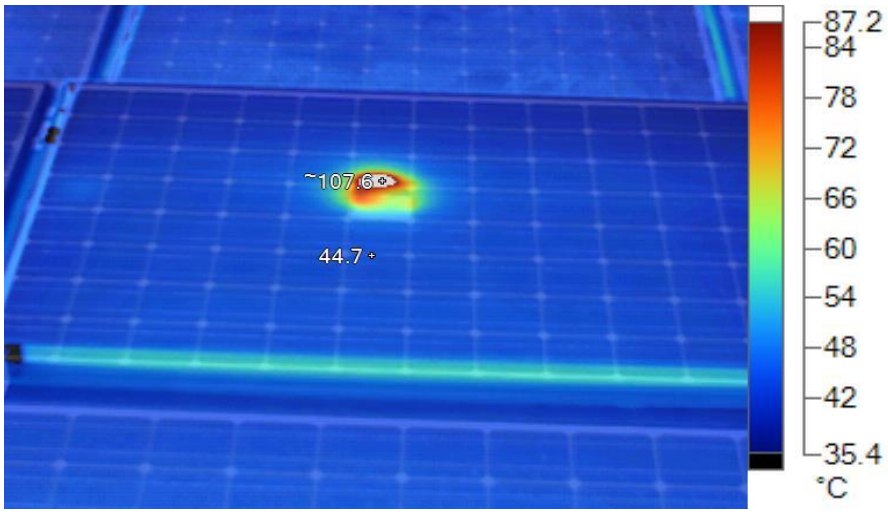

4 IR Image of a Delaminated Cell Creating a Severe Hotspot Causing a Bubble in the Backsheet

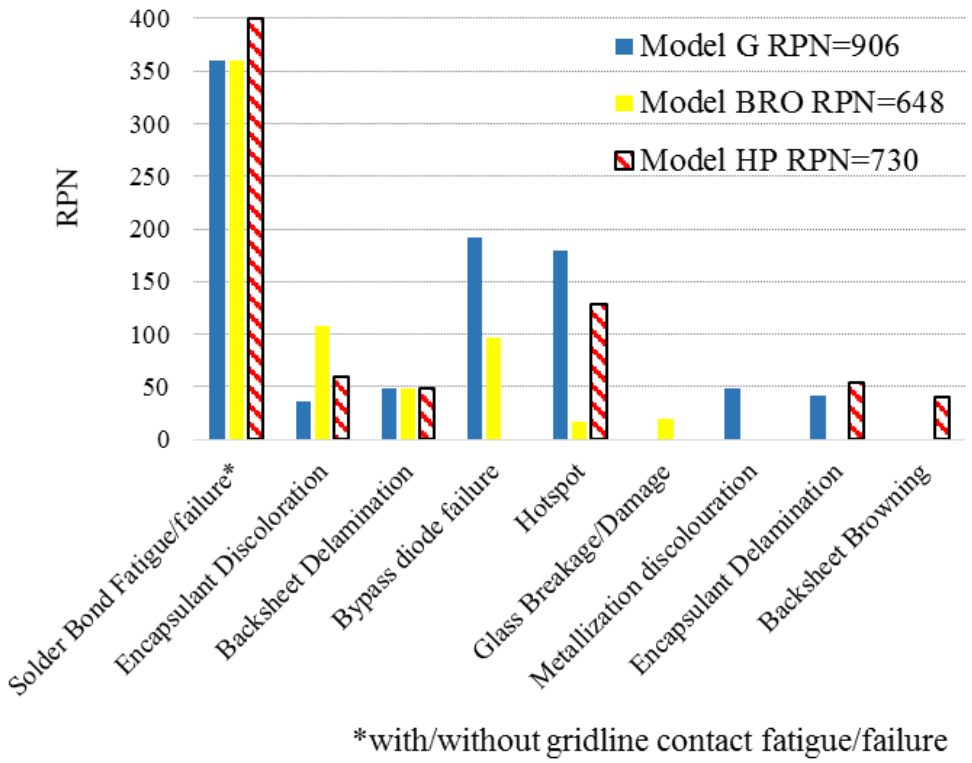

5 RPN vs. Failure Mode of All Three Models Fielded in a Hot-Dry Climate of Arizona

In summary, the RPN of various failure modes of three different sites and three different models in a hot-dry climatic condition of Arizona are shown in Figure 5 and it could be seen that the gridline/metallization contact interface and/or solder bond fatigue/failure (cell/metal and metal/metal interface fatigue/failure) had the highest RPN amongst all the failure modes in all three models.

1.5 CONCLUSION

The occurrence of failure modes of all the three power plants were identified from field evaluation and their severity and occurrence were determined. The FMECA technique was implemented individually to each PV power plant to rank the failure modes according to their impact on the performance and safety of the specific site. Irrespective of the mounting structure of these PV systems in hot and dry climate of Arizona, solder bond fatigue/failure with/without gridline/metallization contact fatigue was found to be the most dominant failure mode in every power plant of this specific climate.

The increase in series resistance of approximately 20% to 40% even in the best modules in all three sites is primarily attributed to solder bond fatigue and/or gridline/metallization interface deterioration. The solder bond and/or gridline/metallization degradation issues, in due course, could progress to failures, and could lead to hotspots or backsheet burns with catastrophic safety failures. Thus it is concluded that the solder bond with/without gridline interface fatigue/failure is the most dominant degradation/ failure mode for these module types under the hot-dry desert climatic conditions irrespective of the construction material type, orientation, and mounting structure of the modules. A deconstructive analysis of these fielded modules is underway in the lab to determine the primary causes and mechanisms for all the failure modes with high RPN values.

PART 2: DETERMINATION OF BEST METHOD TO CALCULATE DEGRADATION RATES

2.1 INTRODUCTION

2.1.1 Background

PV manufacturers typically give a warranty of 20 years to the PV module in the field which implies that the degradation rate of 1%/year is acceptable, if linear degradation is assumed. Thus, the degradation rate is the key measurement to determine the system performance and to project the life time of the project. Manufacturers can determine whether the plant is performing within the warranty limit, has exceeded the warranty limit, or is performing with a high degradation rate but still under the warranty. This study focuses on methods of computing degradation rates of the power plant and determines the optimal method for degradation analyses.

Degradation studies can be carried out from different perspectives such as without irradiance, with irradiance correction [21, 22], IV measurement [1], and so on. The analysis can be modified according to the availability of the data of the site and the installed weather station. Currently, Arizona State University-Photovoltaic Reliability Laboratory (ASU-PRL) evaluated three Salt River Project (SRP) PV power plants for a degradation and reliability study. Among these three sites, two are roof mounted sites and the other is a one-axis horizontal NS tracking site in Arizona. Four different degradation analysis methods discussed in Chapter 3 were implemented in three sites to compute their respective degradation rates, and were compared to I-V measured degradation rates.

2.1.2 Statement of the Problem

The purpose of this thesis is to explain the methodology for obtaining accurate degradation rates of these fielded PV systems. IEC 61724 standard [23] provides an approach of performance ratio to monitor and analyze the photovoltaic system. Wenger 1994 presented a better index for power plant monitoring and analysis for both short term and long term, i.e. a performance index with all the adjustments, losses and gains. ASU-PRL has been using field evaluated IV measurement to determine the degradation rate of the power plants, therefore, this study focuses on different methods discussed above for analyzing accurate degradation rates, and thus, comparing these rates with the degradation rates computed from an ideal IV method measurement.

2.1.3 Objective

The main objectives of this study are to investigate the three PV systems for degradation analysis and they are listed as follows:

- Compute degradation rates from IV measurement, metered raw kWh data, performance ratio, and performance index
- Compare the results from the other three methods to IV measurement degradation rate
- Determine the most optimal method for degradation computation depending upon site's data availability
- Propose an alternative and accurate technique for determination of degradation rate

2.2 LITERATURE REVIEW

2.2.1 PV Array Performance Modelling

Performances of photovoltaic modules depend upon many operating parameters such as irradiance, wind speed, ambient temperature, orientation, mounting structure, BOS, and so on. There are many models within the array performance model that contribute to the overall prediction of performance of the system. Models such as module performance model, irradiance model, thermal model, wiring loss model, soiling model, shading model, etc., within the performance model, are used to determine and predict the performance of the module or system at any given instance. Detailed information about PV array performance modelling can be found in [24, 25].

2.2.2 Thermal Models

Module temperature plays a significant role in the performance, hence, varying the energy production. A 2 deg. C increase in cell temperature corresponds to about a 1% decrease in power; therefore, the prediction of the energy from a large PV power plant depends on the correct prediction of the operating temperature. As of today, there are many thermal models that predict the operating temperature of the PV module in the field such as Sandia, PVSyst, PVSim, ASU-PRL, Duffie & Beckmann models and so on. ASU PRL [26, 27] has developed thermal models for open rack and rooftop systems with different technologies and air gaps, but Sandia's thermal model was used in this study because it covers various types of constructions (glass/glass and glass/polymer) and mounting systems.

2.2.3 Sandia's Thermal Model

King et al [25] developed an empirically-based thermal model. This thermal model applies for flat-plate modules mounted in an open rack, for flat-plate modules on the roof, for flat-plate modules with insulated back surfaces simulating building integrated situations, and for concentrator modules with finned heat sinks. King's paper reported expected module operating temperature with an accuracy of about ±5°C. Temperature uncertainties of this magnitude result in less than a 3% effect on the power output from the module. The model uses two heat transfer coefficients (a, b) derived empirically using thousands of temperature measurements recorded over several different days with the module operating in a near thermal-equilibrium condition. The coefficients determined are influenced by the module construction, the mounting configuration, and the location and height where wind speed is measured. The backsheet temperature of the module is determined using Equation 1:

$$T_m = E * \{e^{a+b.WS}\} + T_a \qquad (4)$$

Where:

T_m = Back-surface module temperature, (°C).

T_a = Ambient air temperature, (°C)

E = Solar irradiance incident on module surface, (W/m^2)

WS = Wind speed measured at standard 10-m height, (m/s)

a = Empirically-determined coefficient establishing the upper limit for module temperature at low wind speeds and high solar irradiance

b = Empirically-determined coefficient establishing the rate at which module temperature drops as wind speed increases

The backsheet temperature and operating cell temperature can be distinctly different, so Equation 2 is used to compute cell temperature from the calculated backsheet temperature assuming one-dimensional thermal heat conduction through the module materials behind the cell.

$$T_C = T_m + \frac{E}{E_0} * \Delta T \qquad (5)$$

Where:

T_c = Cell temperature inside module, (°C)

T_m = Measured back-surface module temperature, (°C).

E = Measured solar irradiance on module, (W/m^2)

E_0 = Reference solar irradiance on module, (1000 W/m^2)

ΔT = Temperature difference between the cell and the module back surface at an irradiance level of 1000 W/m^2. This temperature difference is typically 2 to 3 °C for flat-plate modules in an open-rack mount. For flat-plate modules with a thermally insulated back surface, this temperature difference can be assumed to be zero.

Table 15 shows the empirically-determined coefficients of different module types and mounting configurations. Using these coefficients in Equation 1 & 2, the backsheet and cell temperature can be predicted [25].

15 Empirically Determined Coefficients to Predict Module Back Surface Temperature [25]

Module Type	Mount	a	b	ΔT (°C)
Glass/cell/glass	Open rack	-3.47	-.0594	3
Glass/cell/glass	Close roof mount	-2.98	-.0471	1
Glass/cell/polymer sheet	Open rack	-3.56	-.0750	3
Glass/cell/polymer sheet	Insulated back	-2.81	-.0455	0
Polymer/thin-film/steel	Open rack	-3.58	-.113	3
22X Linear Concentrator	Tracker	-3.23	-.130	13

2.2.4 SolarAnywhere Irradiance Models

In performance modelling, obtaining irradiance data is typically the first step, but in the absence of a ground installed weather station, satellite based weather data plays an important role in the estimation of irradiances. SolarAnywhere [28] generates irradiance estimates using NOAA GOES visible satellite images. The hourly satellite images are processed using the algorithms developed by Dr. Richard Perez [29] at the University of Albany (SUNY). The algorithm extracts cloud indices from the satellite's visible channel using a self-calibrating feedback process that is capable of adjusting for arbitrary ground surfaces. The cloud indices are used to modulate physically-based radiative transfer models describing localized clear sky climatology. SolarAnywhere irradiance estimates have several advantages over ground based measurements including longer histories, lower costs, faster time to market, and the ability to directly produce solar power and variability forecasts. Figure 6 shows the satellite picture used to estimate the irradiance in the SolarAnywhere web based service.

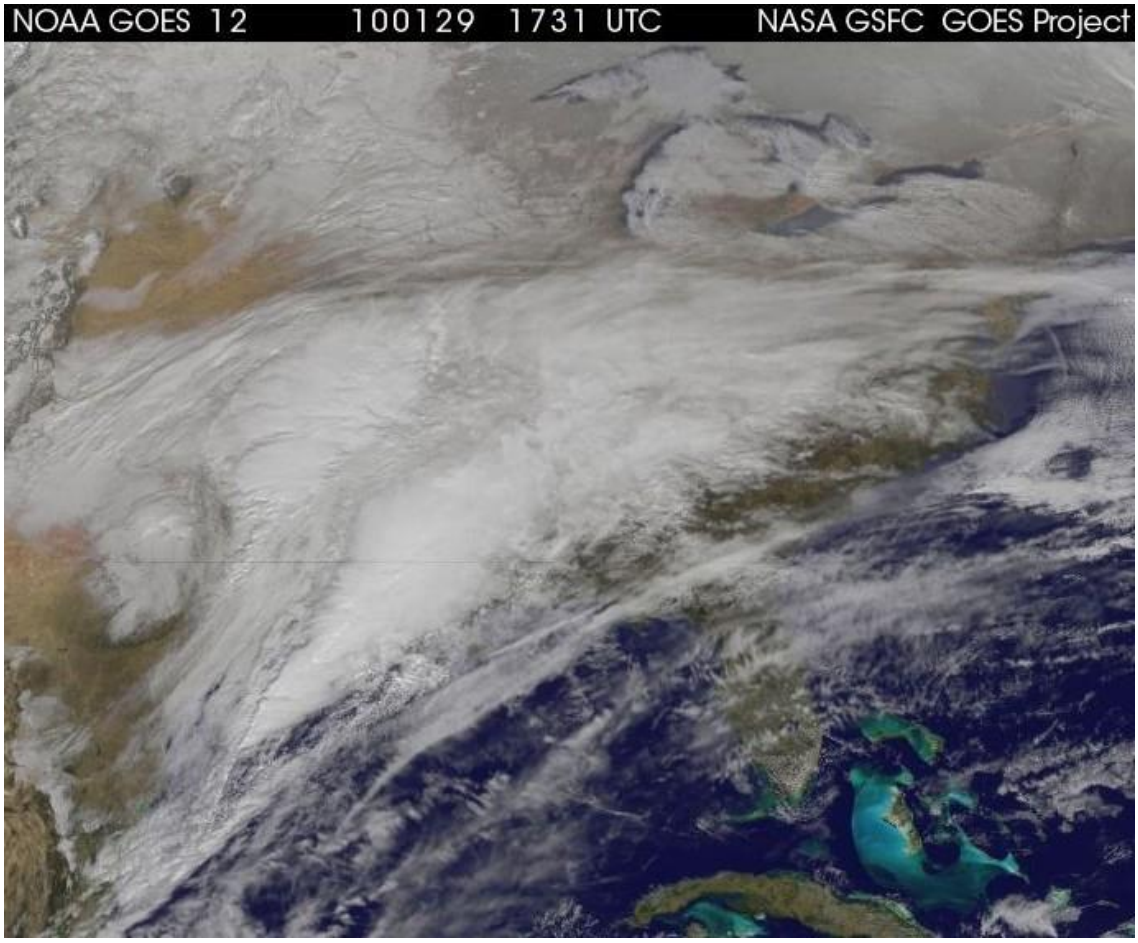

6 Satellite Image for Irradiance Estimation [28]

Whenever there is modelling, uncertainities come to the picture. SolarAnywhere irradiance prediction, using the SUNY model, is believed to be the most accurate source for US satellite derived solar irradiance data. The standard uncertainity for typical sites is around 5%, 10% and 15% for predicted GHI, DNI, and DIF respectively. Figure 7 shows the plot between modelled GHI and measured GHI in Albuquerque in 1999, which shows that there are some uncertainities in the prediction compared to the modelled irradiance. SolarAnywhere web database provides irradiance and weather data for two types of datasets and they are 1X1 km resolution data and 10X10 km resolution data for the US

from 1998 to present. Detailed information about the irradiance model used in this prediction and its validation can be found in Perez et al [29].

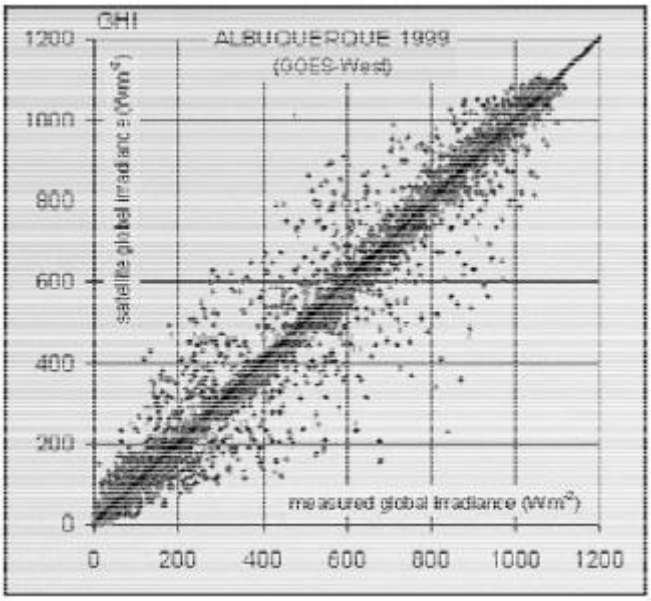

7 Satellite Based Modelled GHI vs. Measured GHI in Albuquerque, 1999 [29]

2.2.5 POA Irradiance Model

Computing the Plane of Array (POA) irradiance is a fundamental step in calculating PV performance [24]. This POA irradiance is dependent upon several factors, including:

- Sun Position
- Array Orientation (Fixed or Tracking)
- Irradiance Components (Direct and Diffuse)
- Ground Surface Reflectivity (Albedo)
- Shading (Near and Far Obstructions)

Equation 6 shows the mathematical form of POA irradiance, E_{POA}:

$$E_{POA} = E_b + E_g + E_d \qquad (6)$$

Where,

E_b = POA beam component = $\mathrm{DNI} * \cos(\mathrm{AOI})$ (7)

E_g = POA ground-reflected component = $\mathrm{GHI} * \mathrm{albedo} * (1 - \cos(\theta_T)/2$ (8)

E_d = POA sky-diffuse component

AOI = Angle of incidence between the sun and the plane of the array

Cos (θ_T) = Surface tilt

Beam and ground-reflected components are straight forward calculations as seen in Equation 7 & 8 respectively; however, the POA Sky Diffuse component is typically divided into several components from the sky dome:

- Isotropic component, which represents the uniform irradiance from the sky dome;
- Circumsolar diffuse component, which represents the forward scattering of radiation concentrated in the area immediately surrounding the sun;
- Horizon brightening component.

Also, there are many models for calculating the POA sky-diffuse component such as:

- Isotropic Sky Diffuse Model
- Simple Sandia Sky Diffuse Model
- Hay and Davies Sky Diffuse Model
- Reindl Sky Diffuse Model
- Perez Sky Diffuse Model

2.2.6 Perez Sky Diffuse Model

This model is considered to be the most accurate sky diffuse model available in the industry as most of the performance model software like PVSyst uses this in the simulation. The basic form of the model is given by Equation 9 [24]:

$$E_d = DHI * [(1 - F_1)\left(\frac{1+\cos\theta_T}{2}\right) + F_1 * \frac{a}{b} + F_2 * \sin\theta_T] \quad (9)$$

Where

F_1 and F_2 are complex empirically fitted functions that describe circumsolar and horizon brightness, respectively

a=max (0, cos (AOI))

b=max (cos (85), cos (θ_Z))

DHI = diffuse horizontal irradiance

θ_z = solar zenith angle

$$F_1 = \max\left[0, \left(f_{11} + f_{12}\Delta + \frac{\pi\theta_z}{180^\circ} f_{13}\right)\right]$$

$$F_2 = f_{21} + f_{22}\Delta + \frac{\pi\theta_z}{180^\circ} f_{13}$$

The f coefficients are defined for specific bins of clearness (ε), which is defined as:

$$\varepsilon = \frac{\frac{DHI + DNI}{DHI} + k\theta_z^3}{1 + k\theta_z^3}$$

Where,

k= 1.041 for angles are in radians (or $5.535 * 10^{-6}$ for angles in degrees)

$$\Delta = \frac{DHI * AM_a}{E_a}$$

Where, AM_a is the absolute air mass, and E_a is extraterrestrial radiation.

Table 16 shows the f coefficient values for irradiance and the ε bin refers to bins of clearness, ε, defined in Table 17. More information about this Perez Sky Diffuse Model can be found in [30].

16 Perez Model Coefficient for Irradiance [28]

ε bin	f11	f12	f13	f21	f22	f23
1	-0.008	0.588	-0.062	-0.06	0.072	-0.022
2	0.13	0.683	-0.151	-0.019	0.066	-0.029
3	0.33	0.487	-0.221	0.055	-0.064	-0.026
4	0.568	0.187	-0.295	0.109	-0.152	-0.014
5	0.873	-0.392	-0.362	0.226	-0.462	0.001
6	1.132	-1.237	-0.412	0.288	-0.823	0.056
7	1.06	-1.6	-0.359	0.264	-1.127	0.131
8	0.678	-0.327	-0.25	0.156	-1.377	0.251

17 Sky Clearness Bins [30]

ε bin	Lower Bound	Upper Bound
1 Overcast	1	1.065
2	1.065	1.230
3	1.230	1.500
4	1.500	1.950
5	1.950	2.800
6	2.800	4.500
7	4.500	6.200
8 Clear	6.200	–

2.2.7 Performance Ratio (PR)

As per IEC 61724 Standard [23], performance ratio (PR) is the ratio of PV system yield, Y_f and reference yield, Y_r. Equation 10, 11 & 12 gives the total system yield, reference yield, and performance ratio, respectively. The performance ratio indicates the overall effect of losses on the array's rated output due to array temperature, incomplete utilization of the irradiation, and system component inefficiencies or failures.

$$Y_f = \tau_R * \frac{\sum P_A}{P_0} * \eta_{load} \quad (10)$$

$$Y_r = \tau_R * \frac{\sum G_I}{G_{I,ref}} \quad (11)$$

$$PR = \frac{Y_f}{Y_r} \quad (12)$$

Where,

$\tau_R * \Sigma P_A$ = daily array energy of the system

P_0 = rated array power

η_{load}= efficiency with which the energy from all sources is transmitted to the loads

$\tau_R * \Sigma G_I$ = daily energy incident on the system

$G_{I, ref}$ = reference irradiance, 1000 W/m^2

2.2.8 Performance Index (PI)

Performance Index (PI) is the enhancement of the performance ratio with all the adjustments such as losses from temperature, wiring, BOS components, and so on. PI is dimensionless, ranges from 0 to 100%, relies on commonly measured quantities for PV systems, applies to real-time and longer-term analyses, normalizes for rated capacity, and independently adjusts for irradiance, temperature, and as many other power loss or gain mechanisms as the user can quantify [31].

The PI is defined as the ratio of actual to expected energy over any time interval and is shown in Equation 13.

$$\text{PI} = \text{Actual energy}/\text{Adjusted energy} \qquad (13)$$

Where,

Actual energy = measured energy at any given time

Adjusted energy = Rated Power x Adjustments

Equation 13 can be derived to even simpler term for easy computation and the modification is shown in Equation 14.

$$\text{PI} = \frac{\text{Actual Energy} * \text{Rated Irradiance}}{\text{Rated Power} * \text{Actual Insolation} * \text{TA} * \text{DA} * \text{SA} * \text{BOSA}} \qquad (14)$$

Where,

Rated irradiance = 1000 W/m^2 for flat plate modules

Rated power = nameplate power of the array

Actual insolation = total energy incident on the plane of array

TA = Temperature Adjustment

DA = Degradation Adjustment

SA = Soiling Adjustment

BOSA = Balance of System Adjustment

2.3 METHODOLOGY

Three PV power plants in Arizona were analyzed using different methods in this degradation study. The sites used in this study are listed in Table 18 below.

18 PV Systems Information

Site	Model	Technology	Mounting	Location	Commissioned Year	Field Exposed Period	DC Rating (KW)
1	Model G	mono-Si	One-Axis NS Horizontal	Glendale, Arizona	2001	12 years	250
2	Model CT	Poly-Si	Rooftop - 5 deg.	Tempe, Arizona	2004	9 years	100
3	Model HP	a-Si & mono-Si	Rooftop - 10 deg.	Scottsdale, Arizona	2008	5 years	100

Four different approaches were taken for degradation rate computation and they are discussed in the following section.

2.3.1 Module IV Method in the Field

This approach is based on field inspection of the system with individual module IV. The computation of degradation rate is fairly straight forward where the degradation rate is calculated from measured power at present and rated power, and assuming the degradation is linear over time. In this method, all the string IV data of the system is measured at

irradiance > 800 W/m^2 and then individual IV of all the modules from the statistically selected strings are taken and the degradation rate per year of each module is calculated using Equation 15.

$$\text{Degradation rate per year} = \frac{(\text{Pmax drop} * 100)}{(\text{Rated Pmax} * \text{age of operation})} \quad (15)$$

Mean and median degradation rates are calculated by plotting the histogram of all the computed rates excluding modules with safety issues. The flowchart in Figure 1 shows the systematic procedure of degradation rate computation used in this analysis.

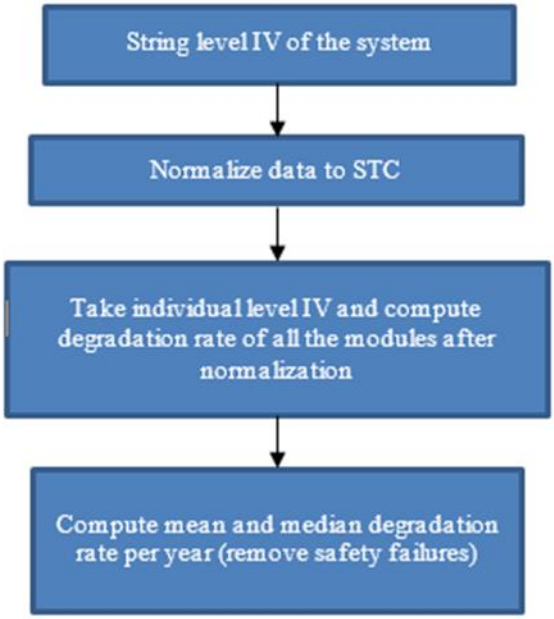

8 Flowchart of Degradation Rate Calculation from IV Measurement

2.3.2 Metered Raw KWh Method

This kWh method uses only metered inverter data to compute the degradation rate without any other data including nameplate data or measured/modeled data for insolation, ambient

temperature etc. This approach avoids the field trips and evaluation completely by just relying on output energy data, which can be collected from a remote server; thus making this method easy, simple and straight forward. A step-by-step process used in this analysis can be shown in Figure 9. Daily energy was calculated and if there were any outliers or flat line data on any day, those days were filtered out in the analysis. Average daily energy of each month was calculated from available days of that month and then, the degradation rate per year of a particular month was calculated assuming the first month energy production is 100%. In this way, 12 degradation rates for 12 months were calculated and finally, mean and median degradation rates of the system were calculated from 12 degradation rates. Belmont et al [22] used metered kWh data to compute the degradation rate of a 26 year old PV system and used regression analysis resulting in only one degradation rate instead of 12 degradation rates for 12 months, which was done in this study.

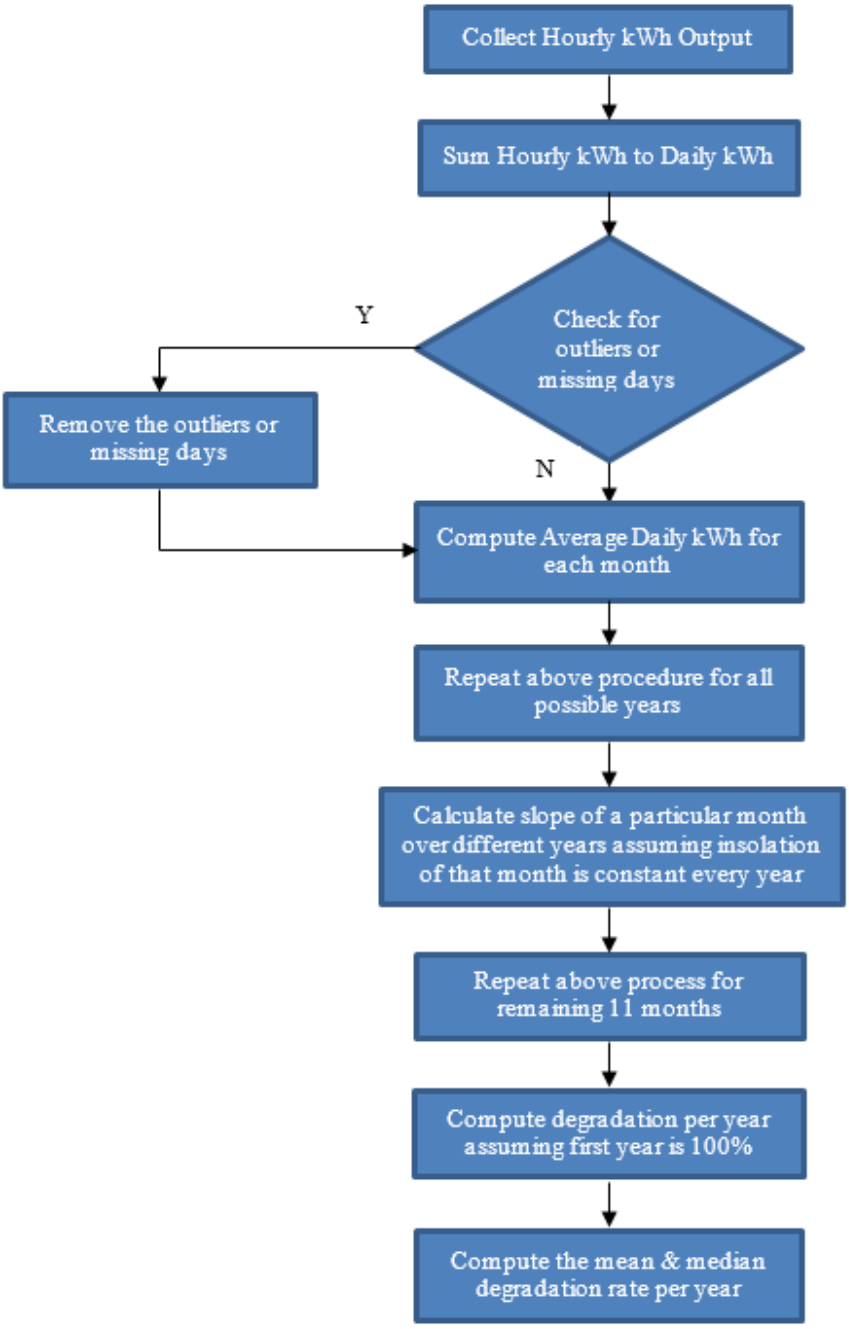

9 Calculation of Degradation Rate per Year Using Just KWh Data i.e. Without Insolation and Temperature Data

This approach can be site specific as the months with high variation in insolation of a site can be avoided in the analysis. Figure 10 shows the variation in monthly insolation from 1991-2010 (data based on NREL-NSRDB, [32]) in Tampa, Florida. This figure shows Oct-Mar in Tampa has high fluctuation in insolation, so the degradation rate per year for this site can be calculated after filtering out those months for better estimation.

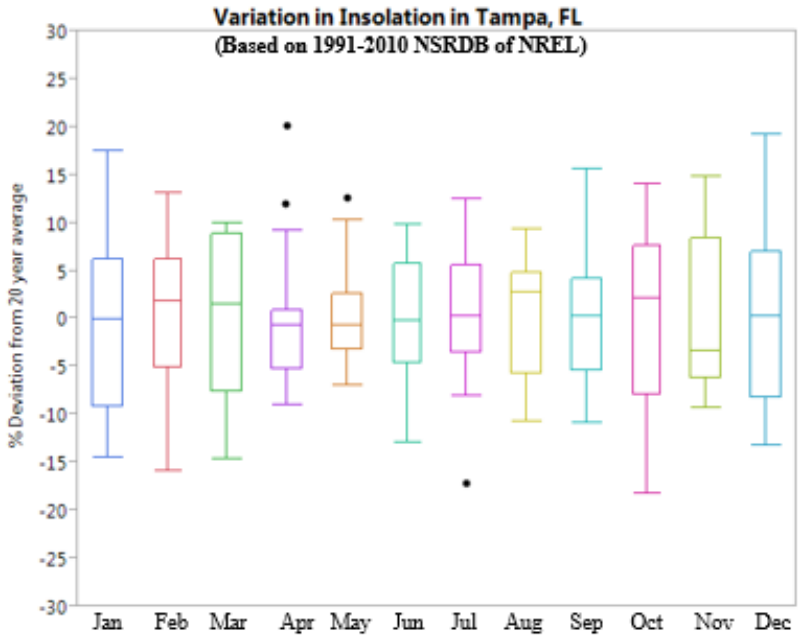

10 Fluctuation in Monthly Insolation from Average Insolation (1991-2010 NREL-NSRDB [32])

2.3.3 Performance Ratio (PR) Method

As discussed in the earlier section, Performance Ratio (PR) is the ratio of measured energy to expected energy based on the nameplate rating and insolation. Daily PR was calculated from measured kWh and calculated expected energy from an irradiance and efficiency of the module. In this study, the insolation data for the site was collected from an installed

local weather station and if it was unavailable, irradiance data was retrieved from SolarAnywhere web database (10X10 km resolution data), which uses Perez's Satellite based model (SUNY model) to predict the Global Horizontal Irradiance (GHI) and Diffused Horizontal Irradiance (DHI). Plane of Array (POA) irradiance of each site, in turn, was computed from the GHI using PVSyst software with Perez's irradiance model. Figure 11 shows the tiles of the sites used from the SolarAnywhere database for weather and irradiance data. The resolution of the tile was 10 km X 10 km and the data was on an hourly basis.

11 Source of Insolation Data (Solar Anywhere Data)

The collected kWh data was filtered out for an irradiance level less than 300 W/m^2 and any flat line data or outliers. This filtration was done to remove spurious data as this method focuses on degradation rate determination. An irradiance level of 300 W/m^2 was chosen as a threshold irradiance level because typically at an irradiance of less than 300 W/m^2,

efficiency of crystalline silicon cells drops leading to data scattering. Also, this level was chosen to avoid any shading phenomenon that can occur early morning or late afternoon when the irradiance level is typically lower than the 300 W/m^2. PR of all the available days was calculated using Equation 16:

$$\mathrm{PR} = (\text{Actual Power})/(\text{Rated Power} * \mathrm{IA}) \quad (16)$$

Where,

IA= Irradiance Adjustment = Actual Irradiance/ Rated Irradiance

PR value of less than 0.5 and greater than 1 were filtered out from the analysis as they are unrealistic for these sites and technologies. Degradation rate of Julian Day 1 was calculated from the slope of computed PR values of the same Julian Day over different operational years. Similarly, 365 degradation rates were calculated for 365 days of a year. Finally, the mean and median degradation rates per year of a system were calculated. The flowchart in Figure 12 shows the step by step procedure to compute the degradation rate using Performance Ratio (PR).

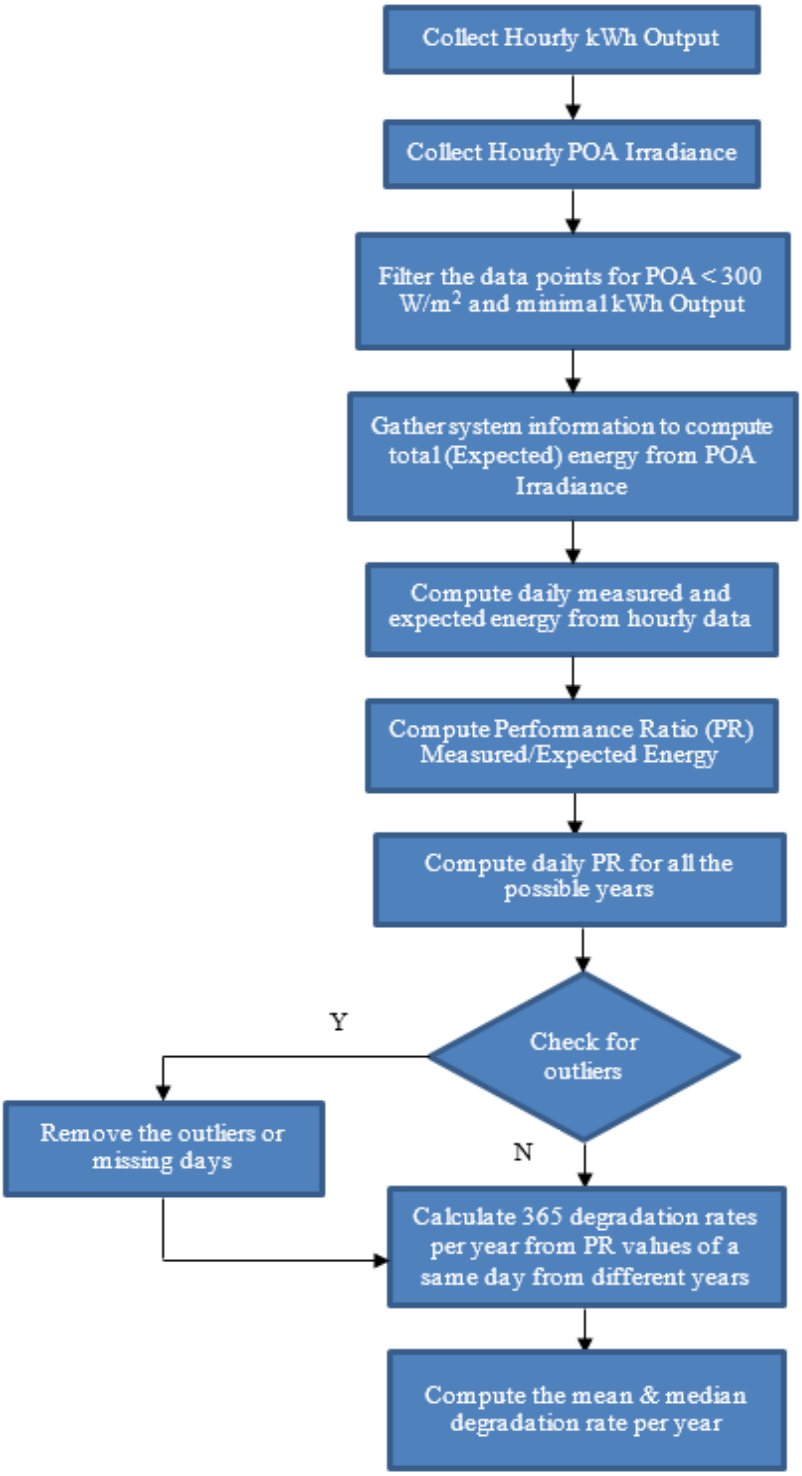

12 Calculation of Degradation Rate per Year Using Performance Ratio (PR) i.e. with Irradiance

2.3.4 Performance Index (PI) Method

Performance Index (PI) is the enhanced version of Performance Ratio (PR) with all the adjustments, so this method is almost identical to the PR method. Performance Index is the ratio of measured energy and expected energy, which is expected energy with all the adjustments such as irradiance, temperature adjustment, electrical losses, and so on. For this analysis, weather data was collected from an installed local weather station and if it was unavailable, irradiance data was retrieved from the SolarAnywhere web database (10X10 km resolution). The module temperature data was calculated and corresponding losses were calculated based on the Sandia's thermal model and PVWatts derate factor [33].

The data was filtered for irradiance < 300 W/m^2 and any flat line data or outliers. This filtration was done to remove spurious data as this method focuses on only degradation rate determination. An irradiance level of 300 W/m^2 was chosen as the threshold irradiance level because typically at an irradiance less than 300 W/m^2, the efficiency of crystalline silicon cells drops, and also to avoid any shading phenomenon that can occur early morning or late afternoon when the irradiance level is typically lower than the 300 W/m^2.

After all these adjustments, daily PI was calculated for all the available days using Equation 17 shown below, and PI values of less than 0.75 and greater than 1.2 were filtered out from the analysis as they seemed unrealistic and outliers for the analysis. The degradation rate of Julian Day 1 was calculated from the slope of computed PI values of the same Julian Day over different operational years. Similarly, 365 degradation rates were calculated for 365 days of a year. Finally, the mean and median degradation rates per year

of a system were calculated. The flowchart in Figure 13 shows the step by step procedure to compute the degradation rate using Performance Index (PI).

$$PI = \frac{\text{Actual Power}}{\text{Rated Power} * IA * TA * BOSA} \quad (17)$$

Where,

IA = Irradiance Adjustment = actual irradiance/rated irradiance

TA = Temperature Adjustment = $1 + \beta*(T_m - 25)$, β = Temperature coefficient, 1/ °C

BOSA = Balance of System Adjustment (from PVWatts)

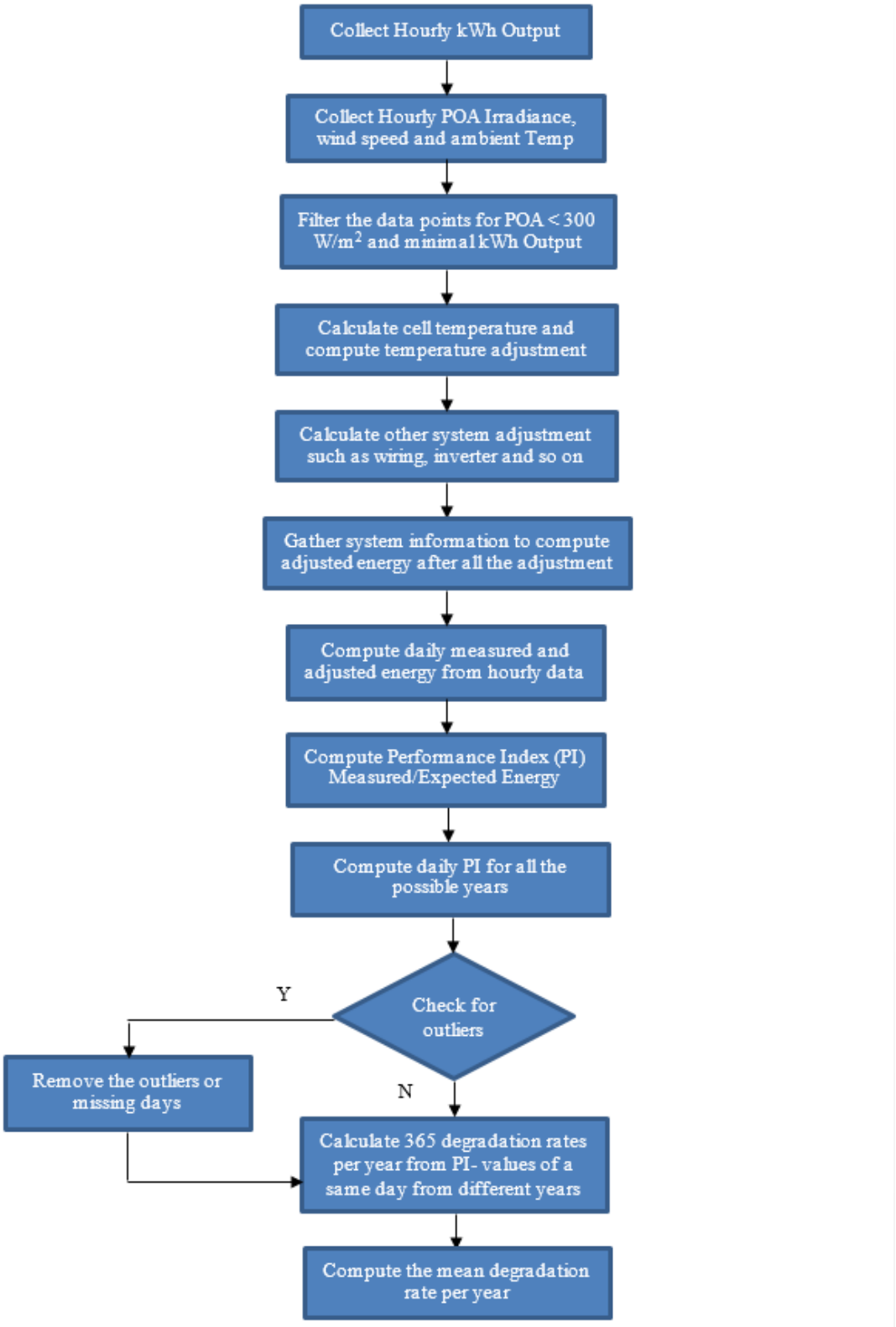

13 Degradation Rate per Year Using Performance Index (PI) i.e. with the Adjustments

2.4 RESULTS AND DISCUSSION

2.4.1 Fielded Module IV Data Analysis

This analysis is based on field trips and individual module IV data collection on a systematically collected sample as discussed in section 3.1. The degradation rate per year of each module was calculated from the formula mentioned in the above chapter. The histogram plots of Model G, Model CT & Model HP are shown in Figures 14, 15 & 16, respectively. From performance measurement, mean and median degradation rates of Model G of -0.95 %/year and -0.96 %/year were calculated respectively with a standard deviation of 0.31 [1]. For Model CT, the mean and median degradation rates were -1.44 %/year and -1.37 %/year with SD of 0.19. Mean and median degradation of Model HP of -1.3 %/year and -0.91 %/year were calculated with SD of 0.4. From the result, median and mean degradation rates of Model HP are not matching, and this is because of the skewness of the data. As discussed in an earlier chapter, all the modules are taken into consideration for degradation rate computation excluding modules with safety failures; therefore, even the worst modules with a high degradation rate but not safety failures are taken into account for this Model HP, which resulted in a high mean degradation rate. In this study, only the median degradation rate is considered as a true representation of the degradation rate, as an average degradation rate can be a skewed value due to the presence of a few, but large, outliers.

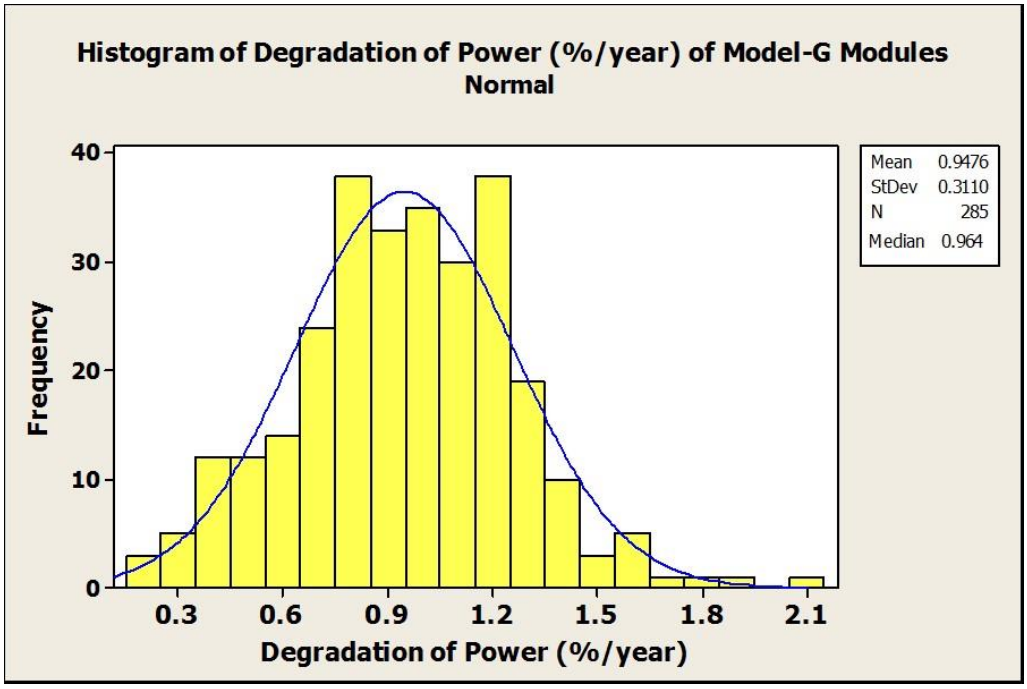

14 Histogram of Model G Degradation per Year Using Performance Measurement (IV) [1]

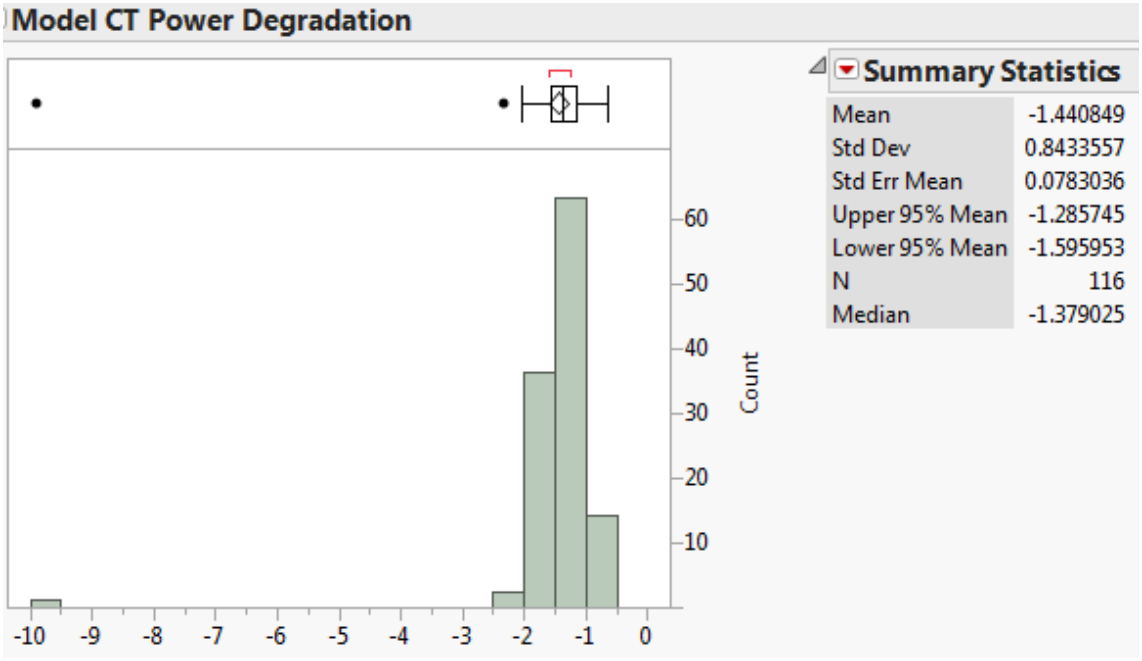

15 Histogram of Model CT Degradation per Year Using Performance Measurement (IV)

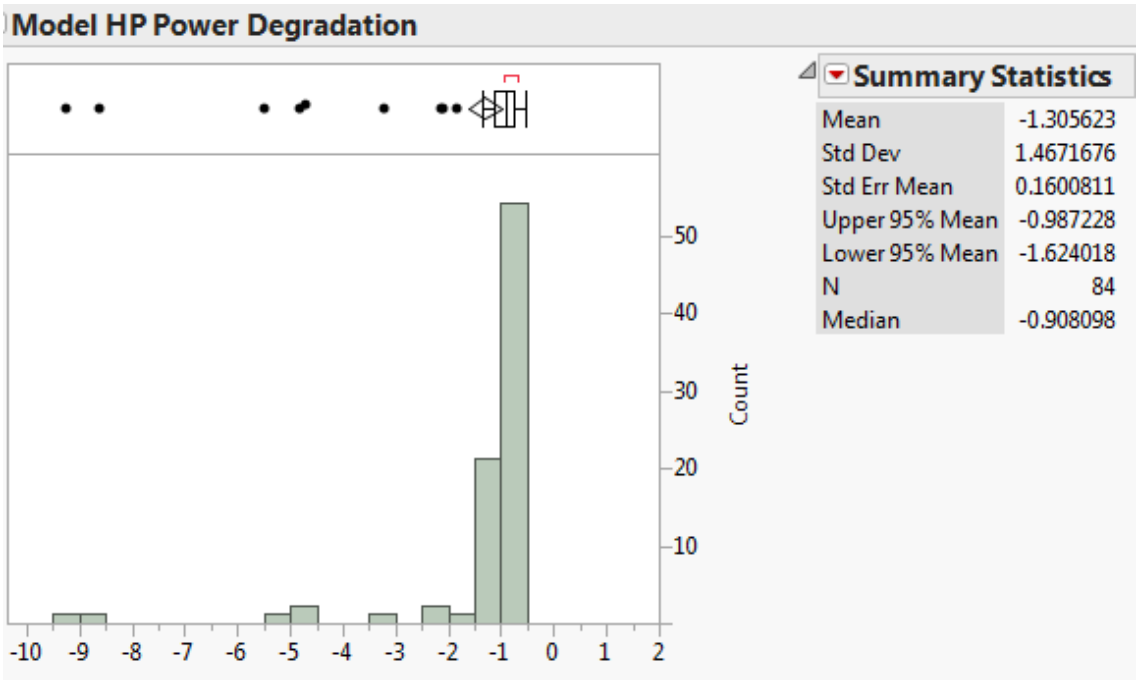

16 Histogram of Model HP Degradation per Year Using Performance Measurement (IV)

2.4.2 Metered Raw Energy (KWh) Data Analysis

In this analysis, only the metered energy (KWh) data was used. Daily average energy for all the months, from installation date to latest date, was computed. The degradation rate of a month was calculated from the slope of average daily energy of the same month over different years, assuming the first month energy production is 100%. The calculation of degradation rate of Model G for the month of April can be seen in the Figure 17. This calculation was repeated for the remaining 11 months for their degradation rates. 12 degradation rates per year for each month were calculated from computing the slope of each month over time and the histograms were plotted for all the sites to compute mean and median degradation rates as shown as in the Figures 18-20.

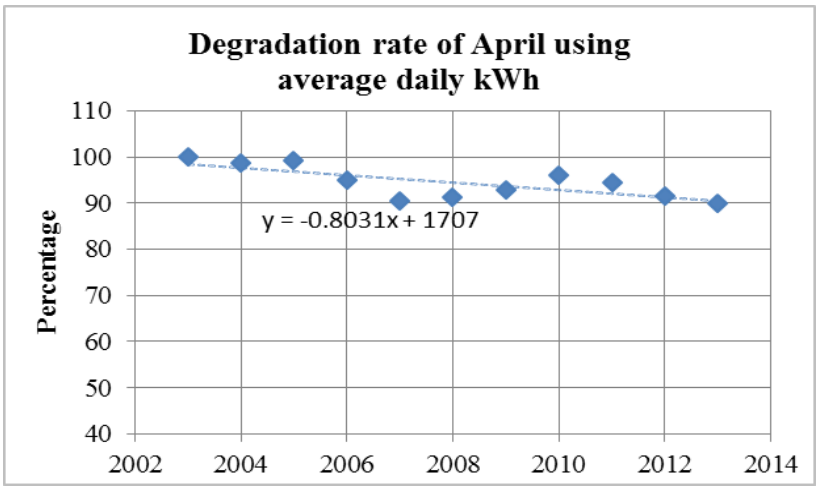

17 Degradation Rate Computation for Month of April for Model G

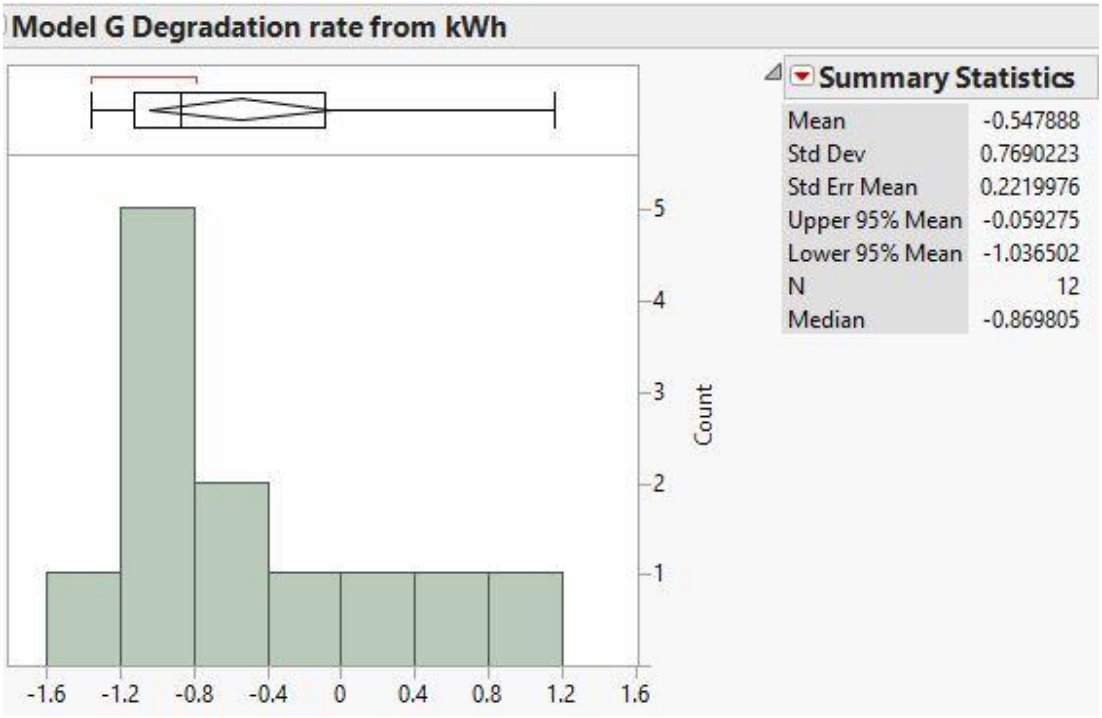

18 Histogram of Model G Raw KWh Degradation Rate per Year

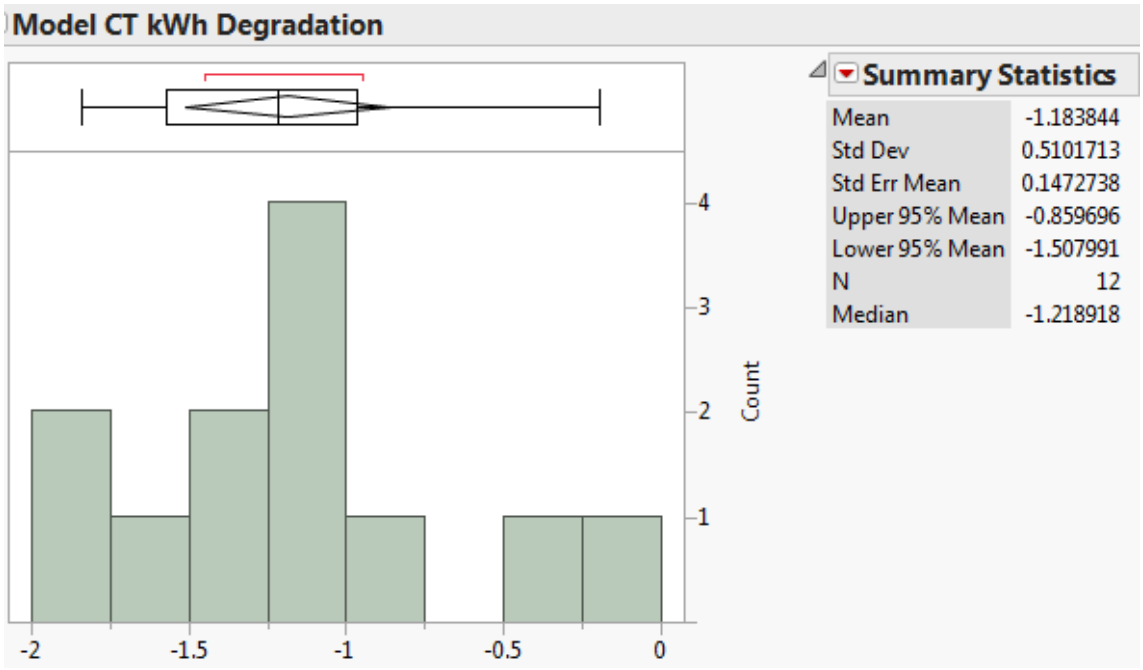

19 Histogram of Model CT Raw KWh Degradation per Year

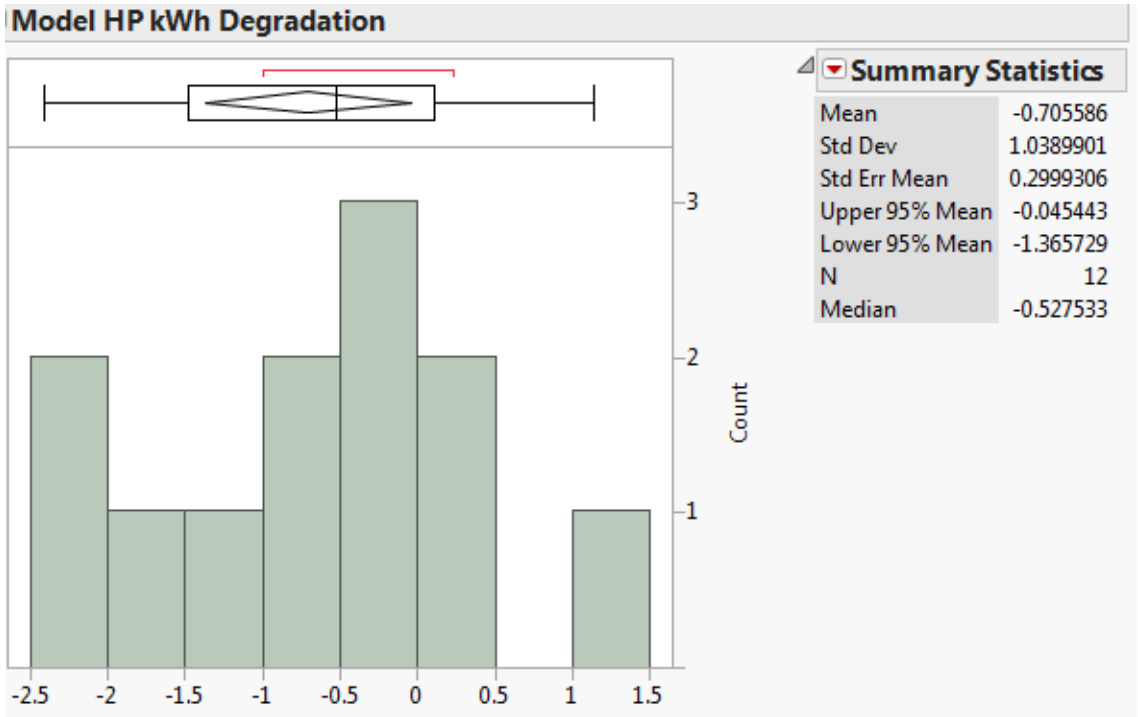

20 Histogram of Model G Raw KWh Degradation per Year

From this analysis, it could be seen that some of the months were having a positive degradation rate which is unrealistic. A detailed look at positive degradation rates for all the three sites in Arizona indicated those months to be around winter time where the variation in insolation is very high and frequent every year. Hence, the fluctuation of monthly insolation from the average insolation of 1998-2013 over different years was computed from the Solar Anywhere data for Phoenix, AZ. Figure 21 shows the box plot of monthly percent deviation in insolation from the average from 1998-2013, and it can be seen that Nov-Mar has more spread and a higher standard deviation.

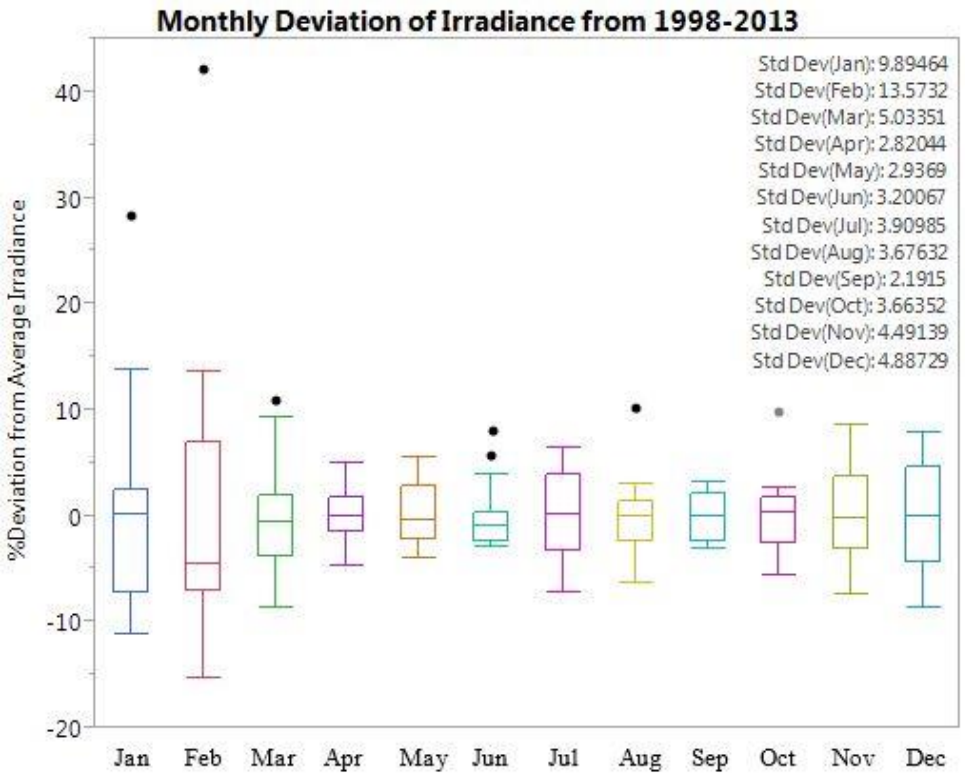

21 Monthly Deviation of Insolation in Phoenix from SolarAnywhere Data (1998-2013)

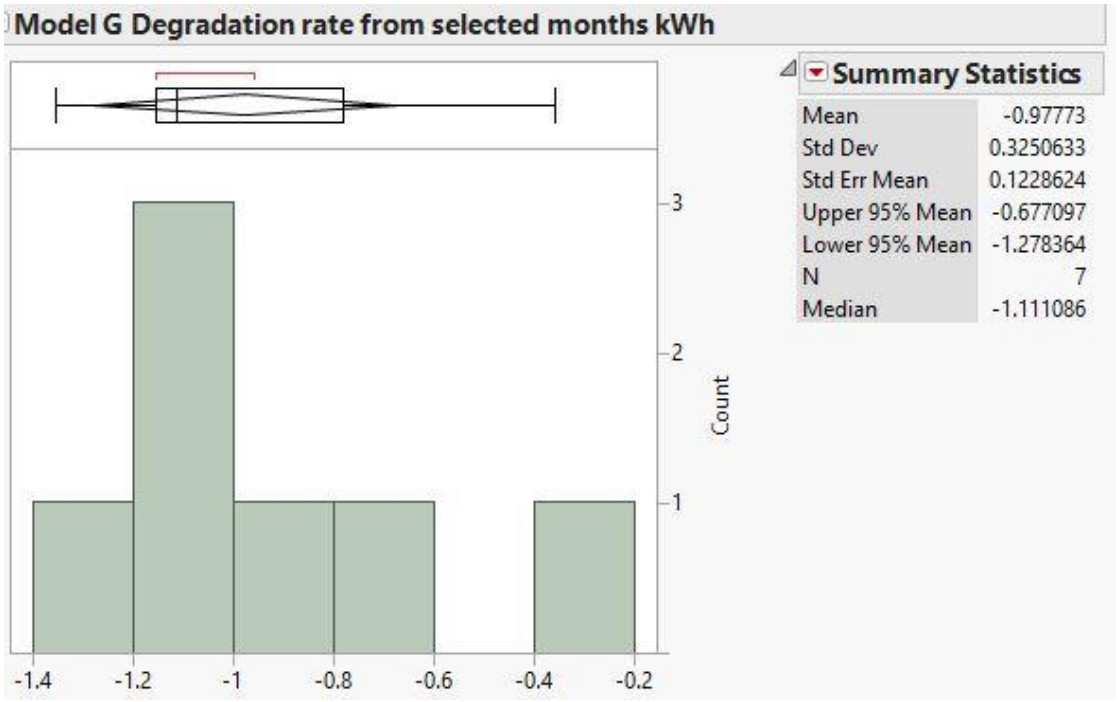

22 Histogram of Model G Degradation per Year Using KWh of 7 Months

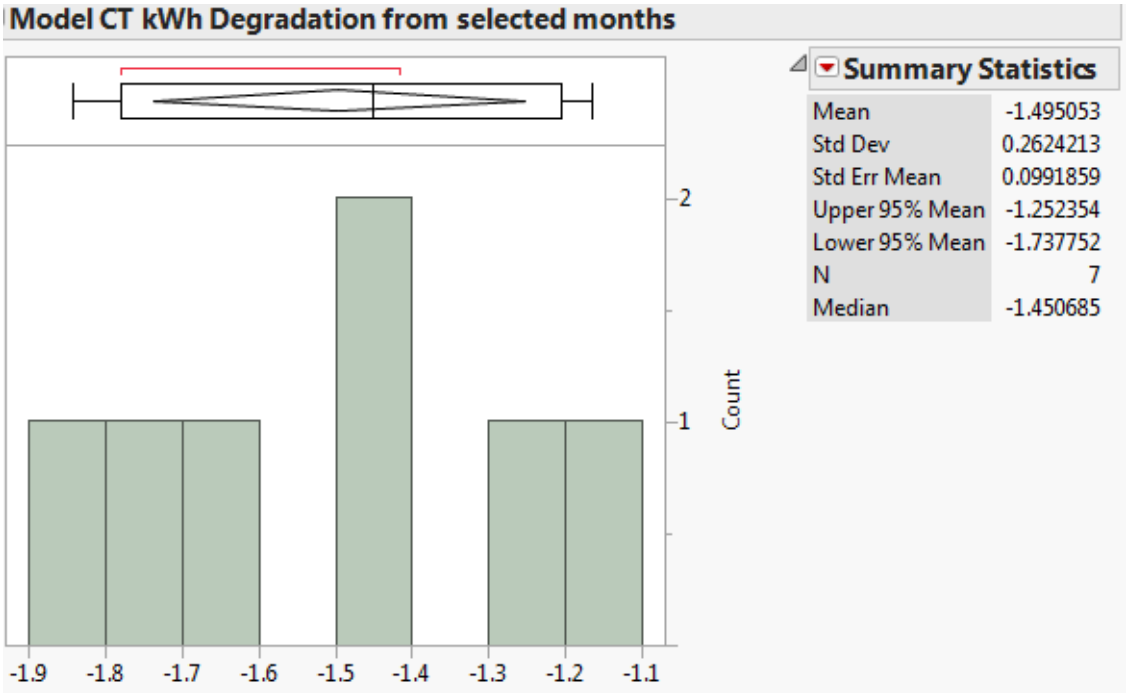

23 Histogram of Model CT Degradation per Year Using KWh of 7 Months

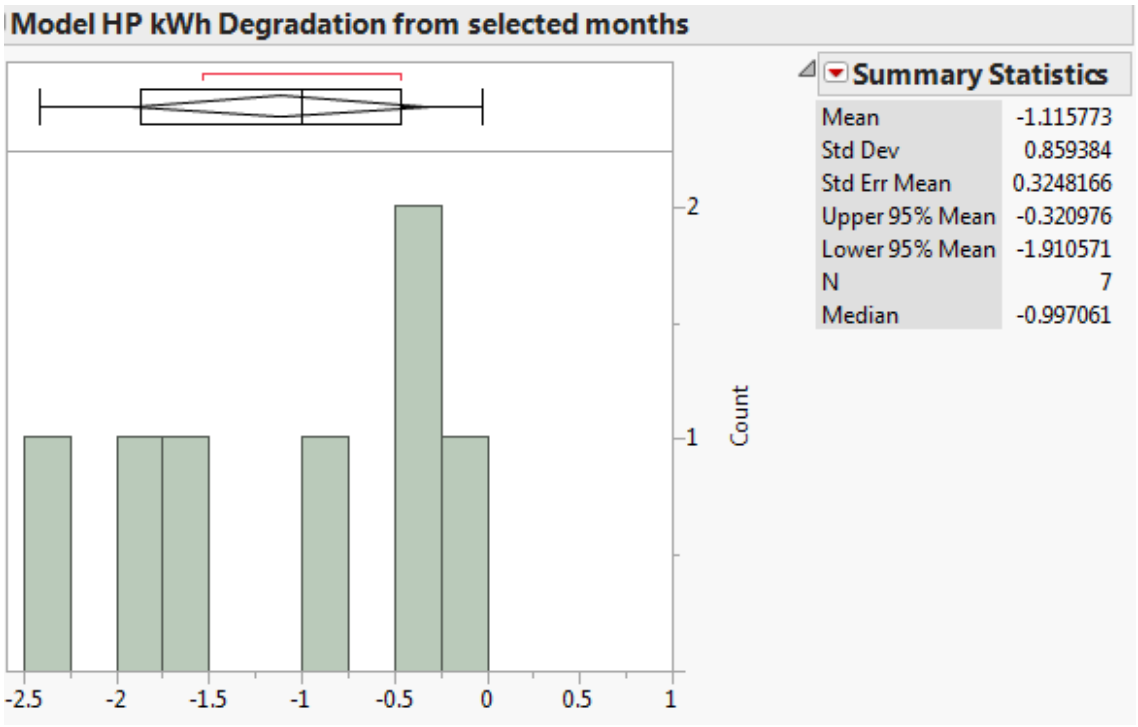

24 Histogram of Model HP Degradation per Year Using KWh of 7 Months

Degradation rates were recalculated after the removal months with high variation in year over year insolation and therefore, only degradation rates of 7 months were used to compute the final degradation rate for these sites in Arizona. Figures 22-24 are the histograms of three sites with only 7 months of degradation rates. From this analysis, mean and median degradation rates of Model G of -0.97 %/year and -1.1%/year were calculated respectively with a standard deviation of 0.32. For Model CT, the mean and median degradation rates were -1.49 %/year and -1.45 %/year with SD of 0.26. Mean and median degradation of Model HP of -1.11 %/year and -0.99 %/year were calculated with SD of 0.4.

In a similar way, this technique can be applied to different sites after determining stable months for each site. Figures 25-28 shows the deviation plot computed from measured

irradiance data from NREL-NSRDB [32] from 1991-2010 for San Diego, Golden, Newark, and Phoenix. To compute degradation rates for these sites, a minimum of 6 good months with less insolation deviation can be picked. For computation of degradation rates, the metered kWh data of the following months are recommended for these sites from Figures 18-21: San Diego, CA - June to November; Golden, CO - May to October; Newark, NJ - April-May & July to October; Phoenix, AZ – April to October.

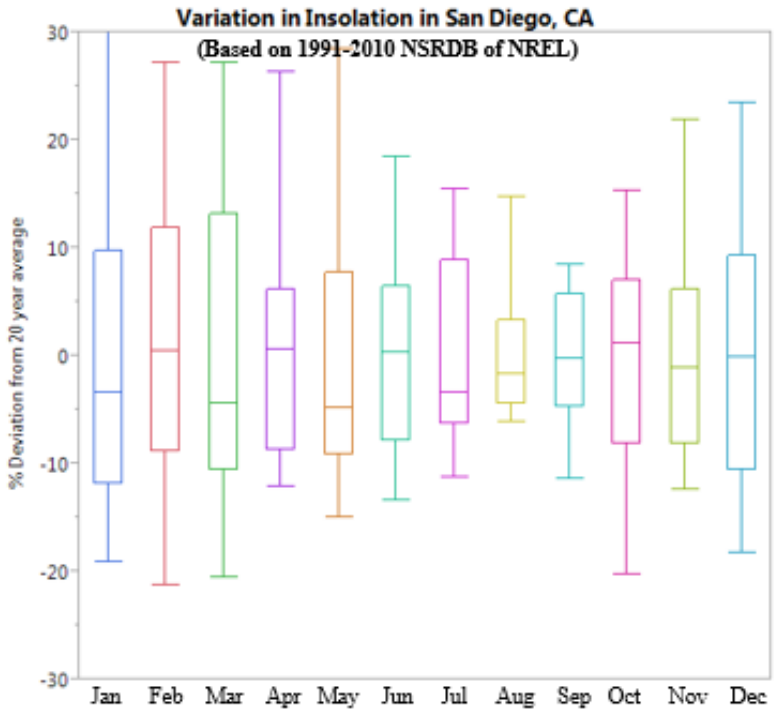

25 Monthly Variation of Insolation in San Diego, CA

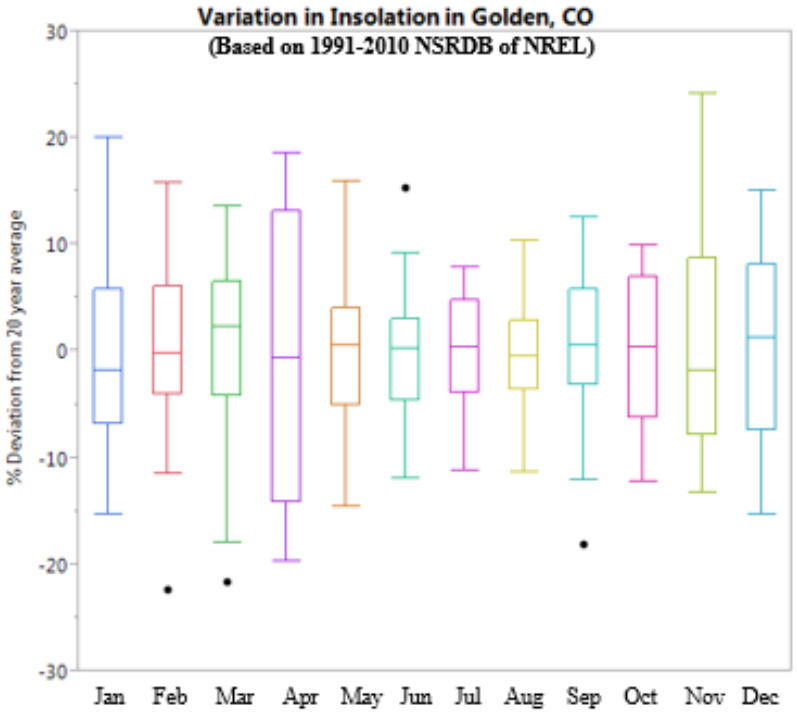

26 Monthly Variation of Insolation in Golden, CO

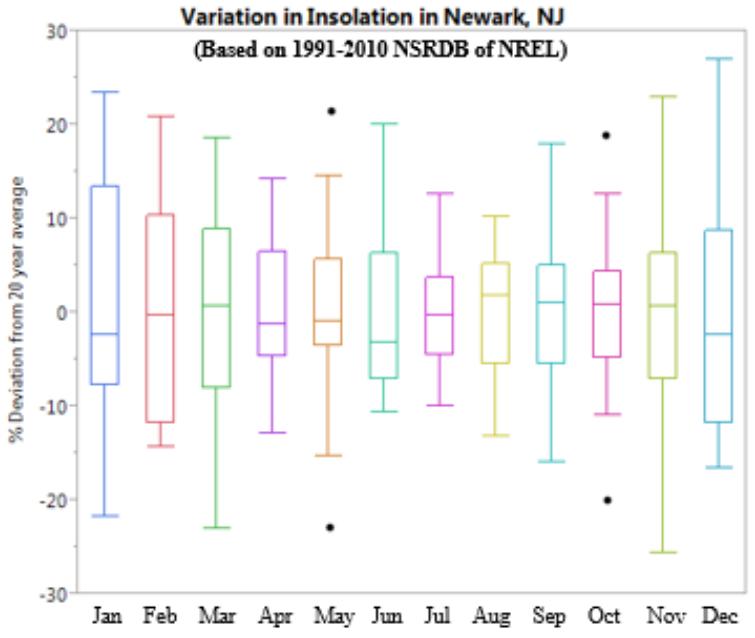

27 Monthly Variation of Insolation in Newark, NJ

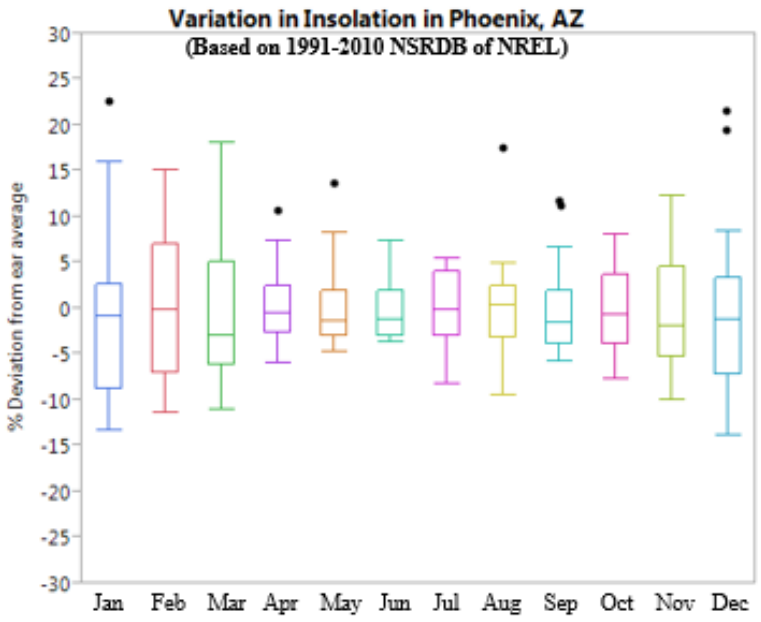

28 Monthly Variation of Insolation in Phoenix, AZ

2.4.3 Performance Ratio (PR) Data Analysis

In this analysis, the daily Performance Ratio (PR) was calculated for all the available days as discussed in the previous methodology chapter. For Model G and CT, only the first 5 years of met station data were available, so for rest of the years SolarAnywhere data was used. Model HP never had installed a weather station, so this site used only modelled data in this analysis. Then, 365 degradation rates were computed from the slope of daily PR of the same Julian days. Figure 29 shows the computation of the degradation rate per year for Julian day 32 (February 1).

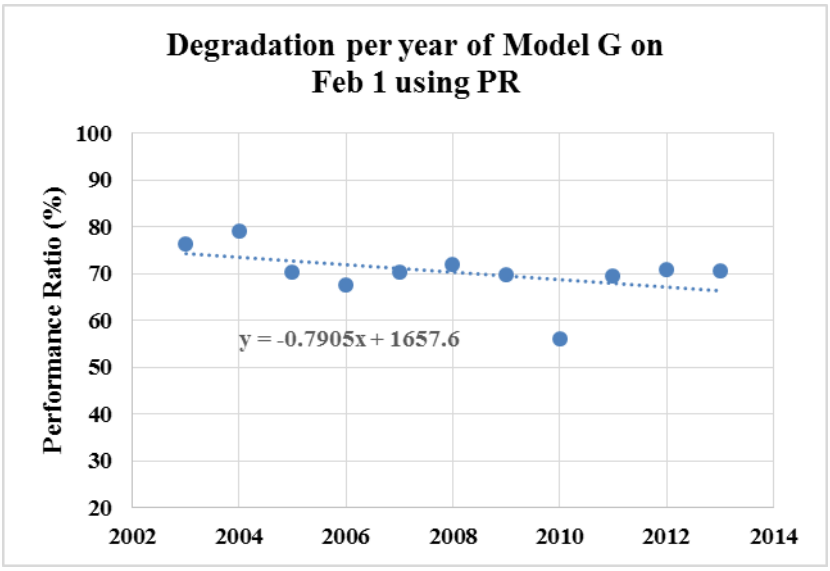

29 Degradation Rate per Year on Feb 1 of Model G Using PR Analysis

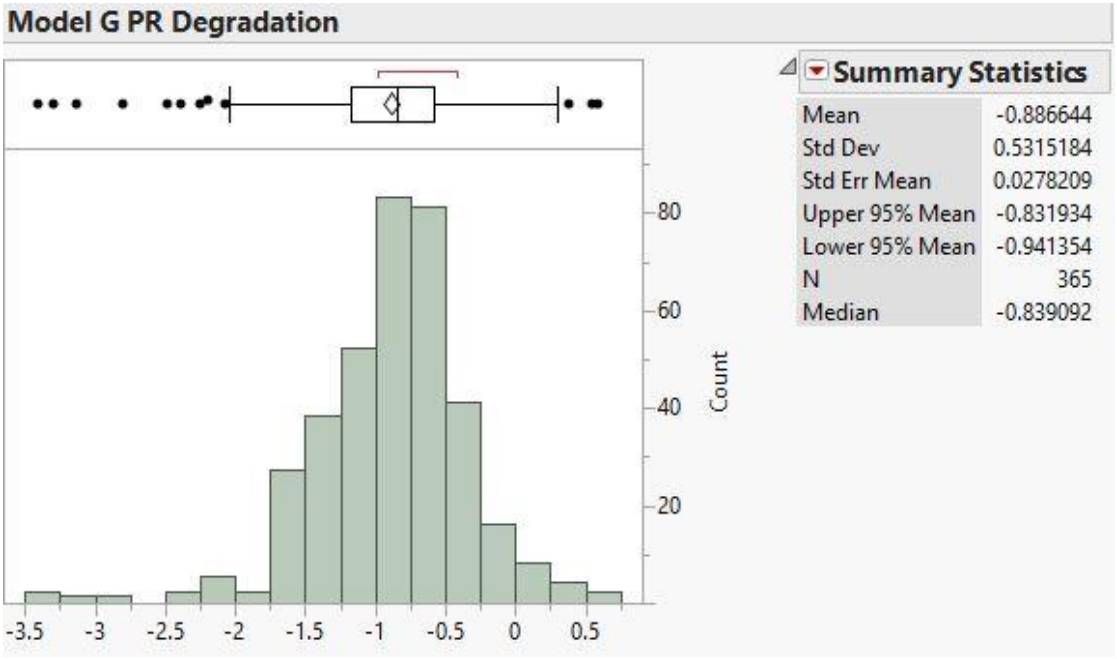

30 Histogram of Model G Degradation per Year Using Performance Ratio (PR)

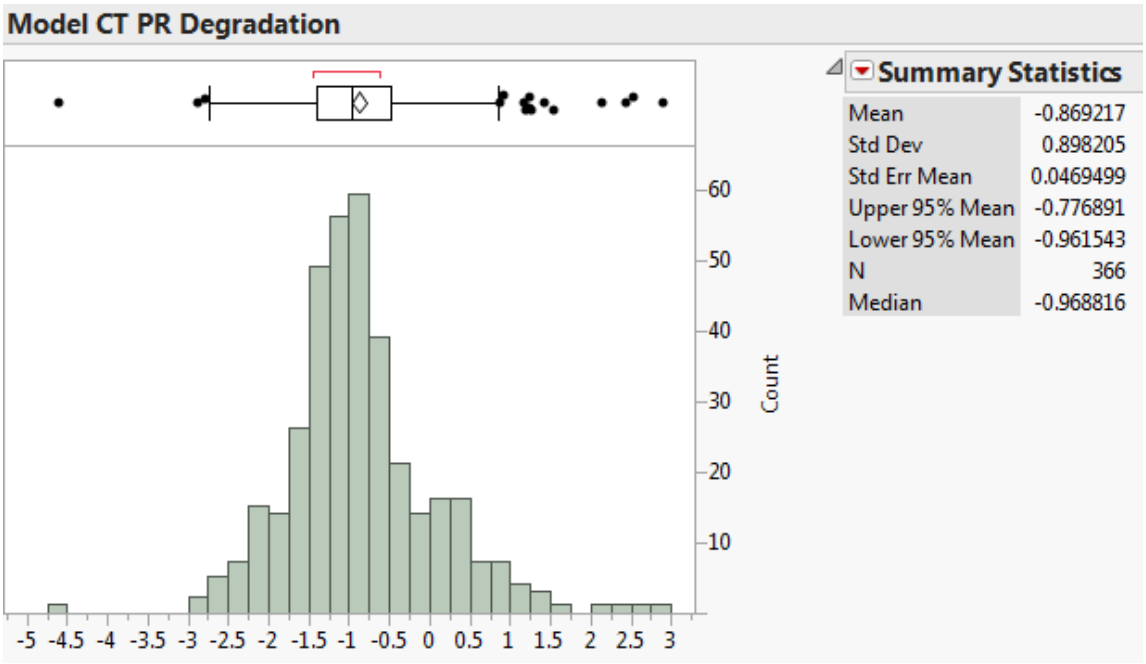

31 Histogram of Model CT Degradation per Year Using Performance Ratio (PR)

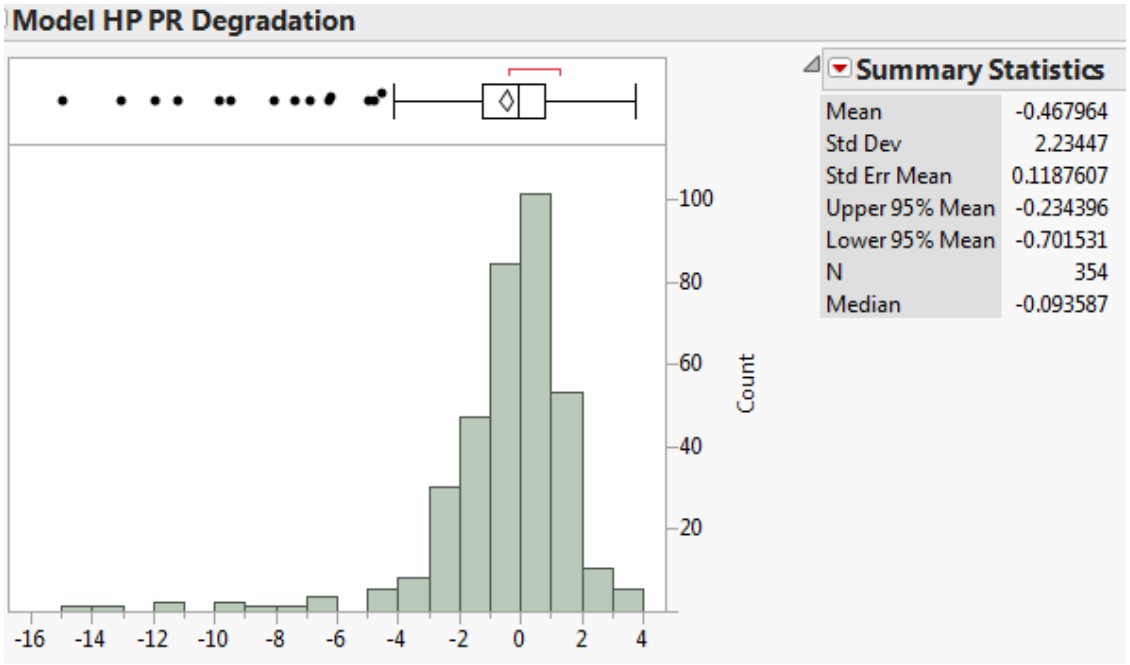

32 Histogram of Model HP Degradation per Year Using Performance Ratio (PR)

365 degradation rates were computed using the PR method for all three sites and the histograms were plotted as shown in Figures 30, 31 & 32 for Model G, Model CT & Model HP, respectively. From this analysis, mean and median degradation rates of Model G of -0.88 %/year and -0.84 %/year were calculated respectively with a standard deviation of 0.58. For Model CT, the mean and median degradation rates were -0.87 %/year and -0.97 %/year with SD of 0.04. Mean and median degradation of Model HP of -0.47 %/year and -0.1 %/year were calculated with SD of 2.23.

2.4.4 Performance Index (PI) Data Analysis

In this analysis, the daily Performance Index (PI) was calculated for all the available days as discussed in the previous methodology chapter. Model HP used SolarAnywhere irradiance and weather data, whereas, Model CT and G used local weather data for the first five years, and then for the rest of the time, it used SolarAnywhere data. For temperature adjustment, the cell temperature was calculated using Sandia's thermal model where open rack coefficients were used for Model G ($a = -3.56$, $b = -0.075$, $\Delta T = 3$, one axis tracker) and rooftop coefficients were used for Model CT & HP ($a = -2.98$, $b = -0.0471$, $\Delta T = 1$, rooftop system). Temperature coefficients of -0.45%/°C, -0.47 %/°C & -0.3%/°C were used for Model G, Model CT & Model HP respectively for the computation for temperature adjustment for PI evaluation. After calculating PI for all the days, 365 degradation rates were computed from the slope of daily PI of the same Julian days. Figure 33 shows the computation degradation rate per year of Julian day 60 (March 1).

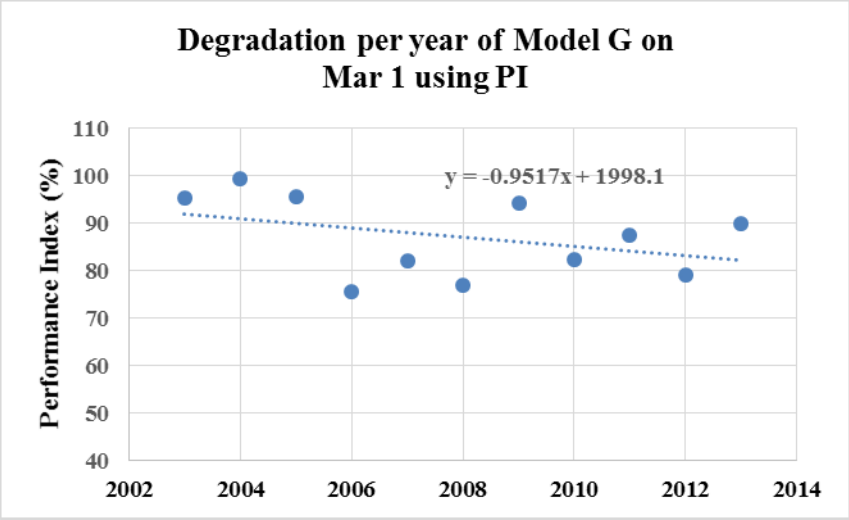

33 Degradation Rate per Year on Mar 1 of Model G Using PI Analysis

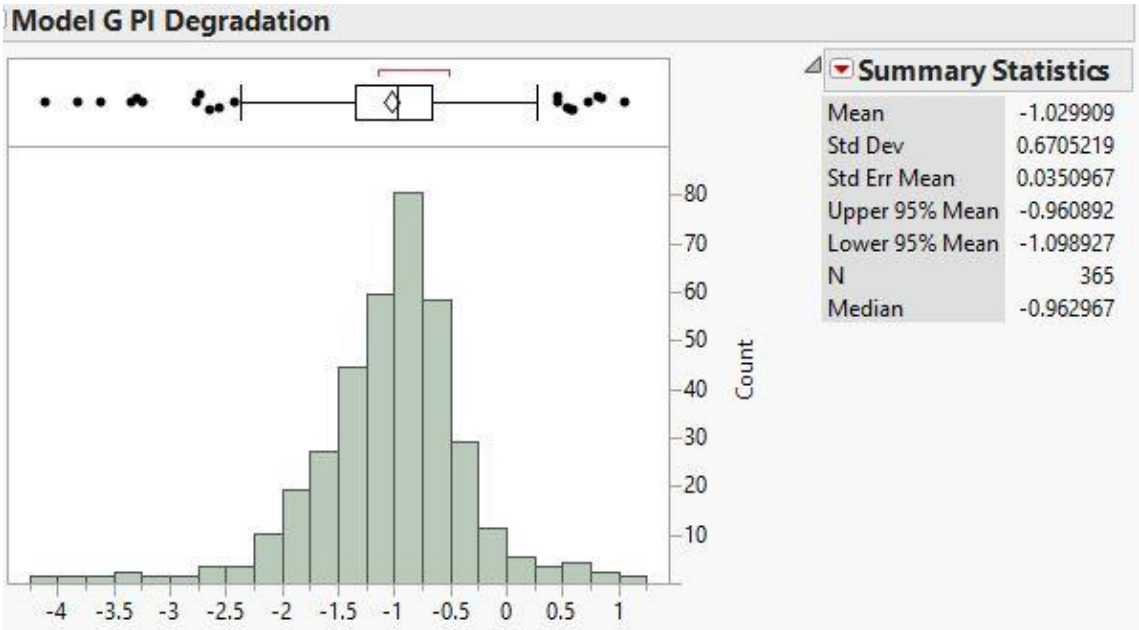

34 Histogram of Model G Degradation per Year Using Performance Index (PI)

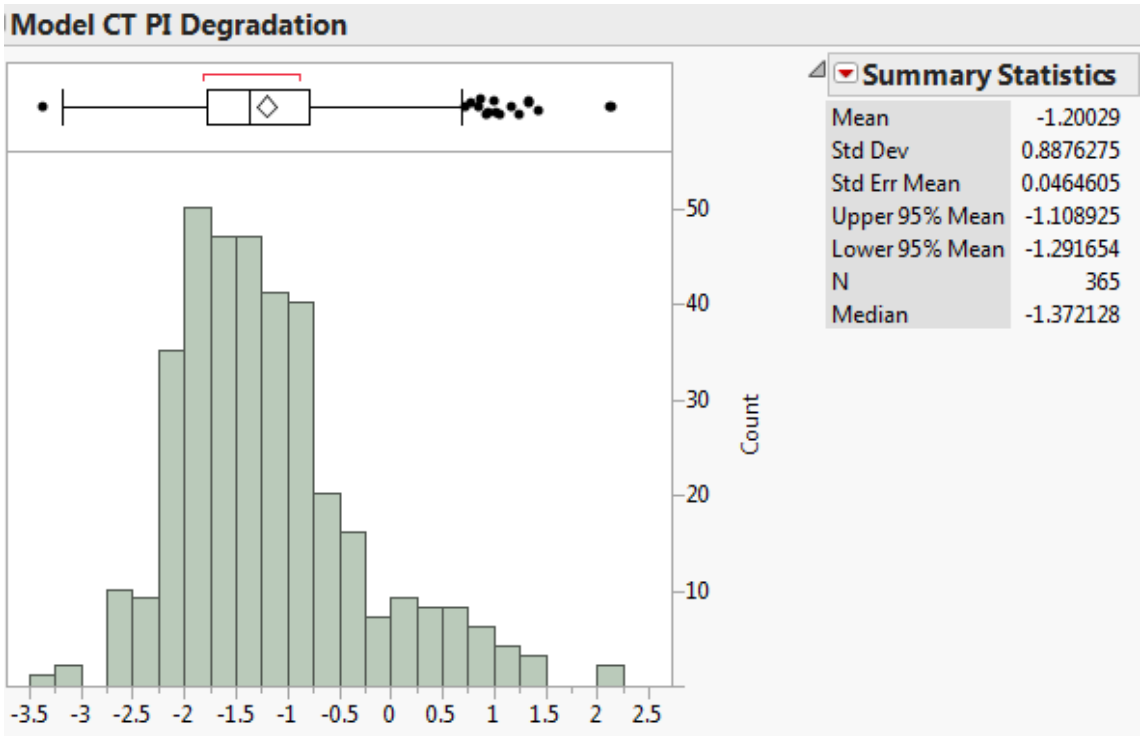

35 Histogram of Model CT Degradation per Year Using Performance Index (PI)

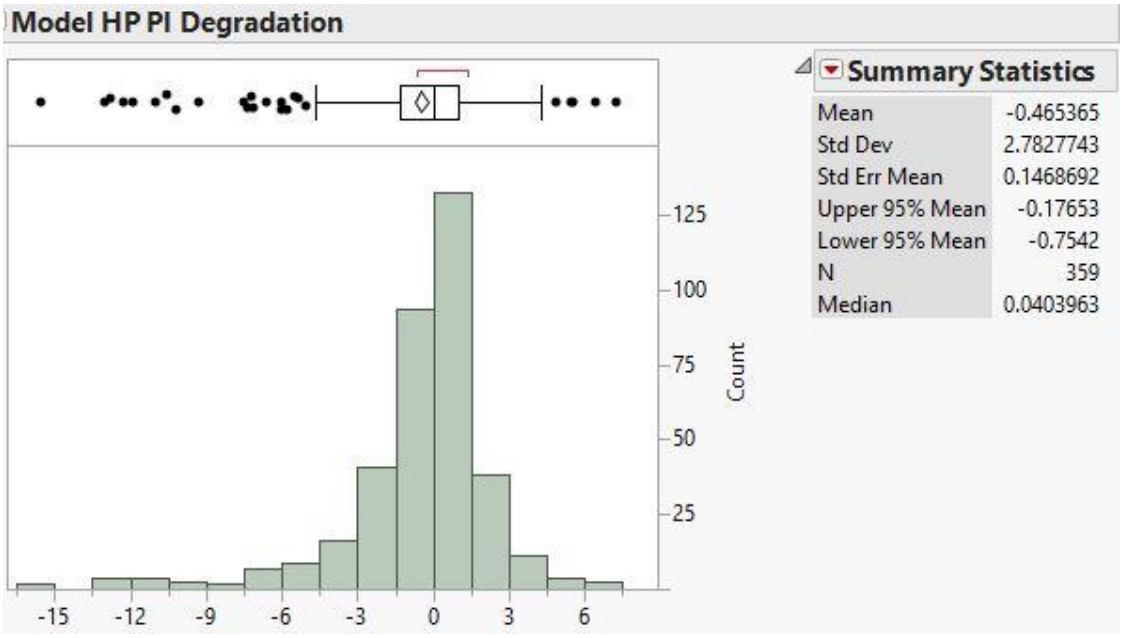

36 Histogram of Model HP Degradation per Year Using Performance Index (PI)

365 degradation rates were computed using the PI method for all three sites and the histograms were plotted as shown in figures 34, 35 & 36 for Model G, Model CT & Model HP, respectively. From this analysis, mean and median degradation rates of Model G of -1.02 %/year and -0.96 %/year were calculated respectively with a standard deviation of 0.67. For Model CT, the mean and median degradation rates were -1.2 %/year and -1.37 %/year with SD of 0.88. Mean and median degradation of Model HP of -0.47 %/year and 0.04 %/year were calculated with SD of 2.78.

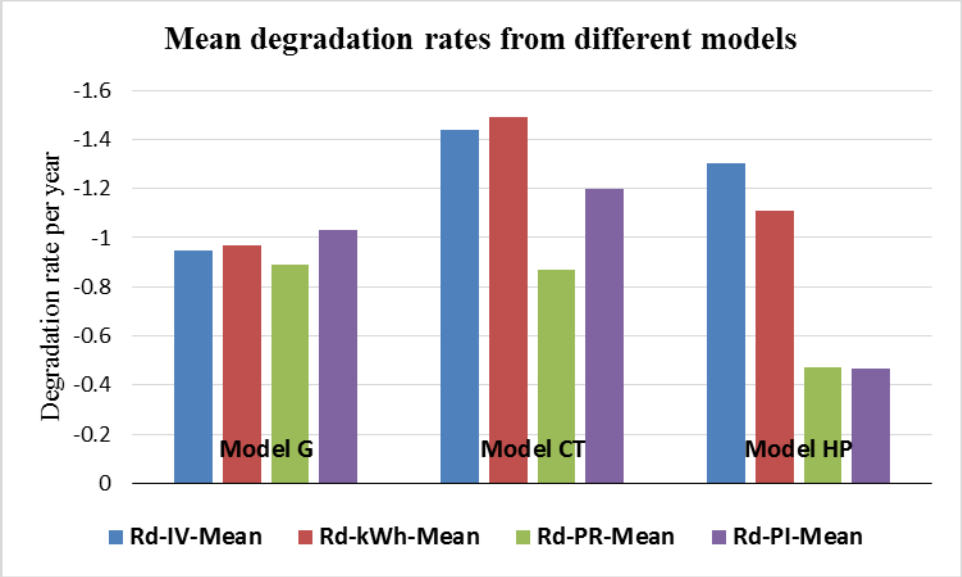

37 Plot of Mean Degradation Rate per Year of Three Models Using Different Methods

Figure 37 and 38 shows the mean and median degradation rates of three sites respectively and the degradation rates evaluated from kWh, PR, & PI are compared with the degradation rate from the I-V measurement. The mean and median degradation rates computed from kWh method for all three models were deviating ±0.15% from the IV measurement degradation rates. Only median degradation rates were used to represent the

true degradation rates of the system as median avoids skewness of the data. Figure 39 shows the percent deviation of degradation rates computed from kWh, PR, and PI method from I-V method for three models, and can be seen that degradation rates computed from the KWh method are fairly accurate.

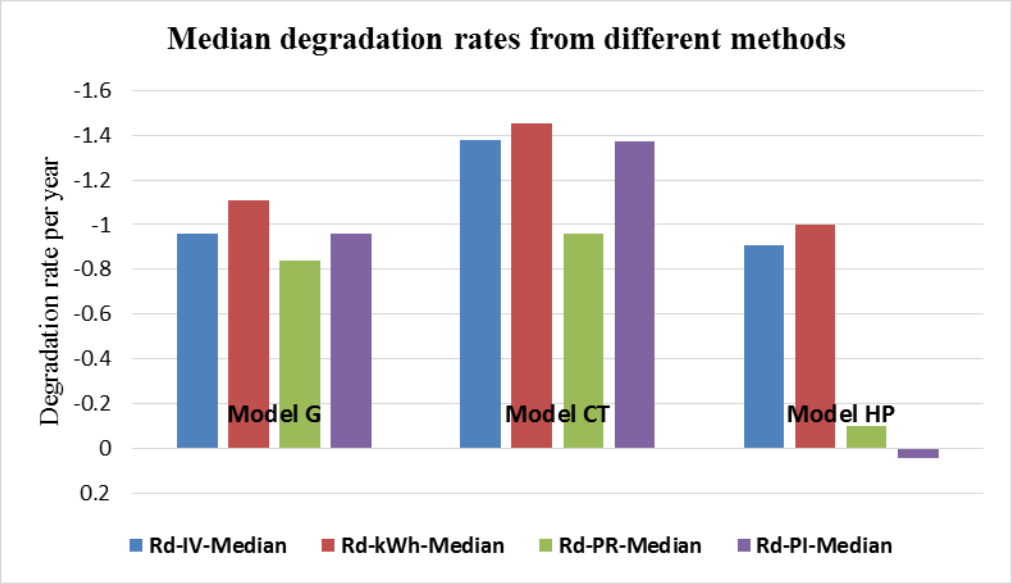

38 Plot of Median Degradation Rate per Year of Three Models Using Different Methods

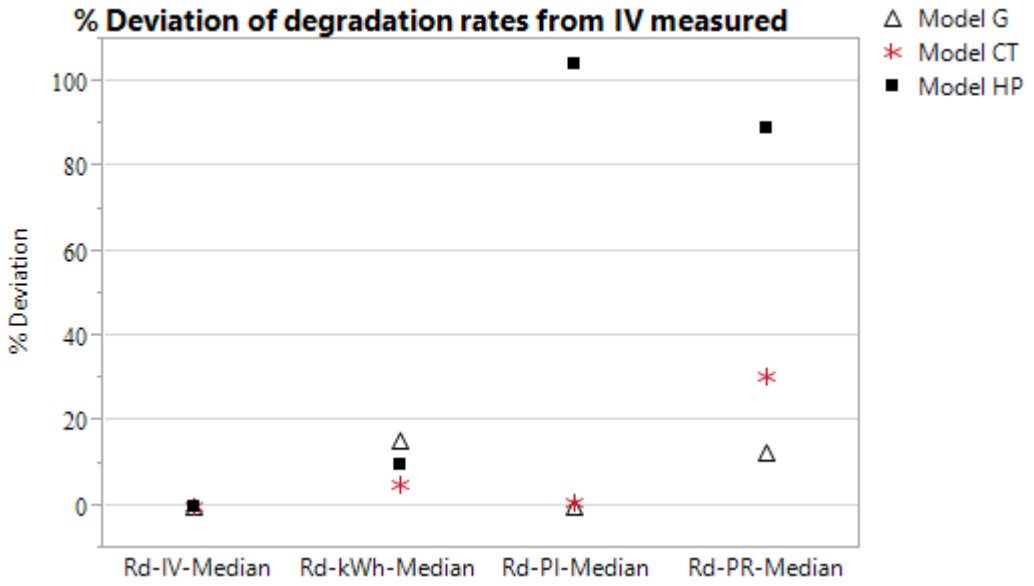

39 Deviation of Computed Degradation Rates from I-V Measured Rate

For CT and HP, the PR method is not working well as seen in Figure 39, because of the high operating temperature of the modules on the rooftop with limited backsheet cooling as they are installed at 5 degree and 10 degree tilts, and also due to dependency on modelled irradiance data. The degradation rates of Model G and CT calculated from the PI method had ±0.02 % deviation from the I-V measured rate, however for Model HP, the deviation was more than 1%. Model CT and G used 5 years of locally measured weather data and 6 and 5 years of satellite data for Model G and CT respectively in this analysis, whereas, Model HP used only satellite modelled data for five years, as there was no ground mount weather data available for this site. In this analysis, 10X10 km resolution satellite based modelled irradiance data from SolarAnywhere was used; however, the accuracy of irradiance data can be improved by using enhanced resolution data of 1X1 km grid from SolarAnywhere. Again, this irradiance was modelled for individual site POA irradiance

using PVSyst's Perez model, and the operating cell temperature was predicted using the modelled irradiance. Therefore, in every step of modelling, there are many uncertainties from these models influencing the result. Also, for rooftop modules, Sandia's thermal model tends to over predict the cell temperature compared to the open rack modules, which affects the predicted performance of the system. Sandia's coefficients for rooftop modules were derived from close roof mount i.e. low standoff mounted modules, but these rooftop systems were having high standoff, which implies that the coefficients might have influenced the predicted cell temperature in thermal modelling, and eventually resulted in a biased degradation rate. Also, the fact that the number of years of operation is less (5 years) for this Model HP site, therefore, less data points are available when calculating the slopes for degradation analysis and might result toward a biased trend.

Performance Index (PI) is a very good measure of instantaneous performance as well as a good index for degradation calculation as it has been used widely in the industry, however, the cost of installing and maintaining a weather station for POA irradiance, ambient temperature and wind speed for an individual site should make financial and economic sense to the size. In addition, day-to-day maintenance of a MET station of the site can be time consuming and expensive, and depending on satellite weather data for performance and degradation computation, it can produce a biased result. However, if the systems are in megawatts, it is viable to have an individual, well-maintained weather station so that the PI computation will help in instantaneous performance monitoring as well as long term analysis such as degradation, soiling, and so on.

Field evaluation with IV measurement is the ideal and most accurate method for degradation calculation, however, the time and effort to apply this process in the field is high, which makes it difficult for the larger systems. On the other hand, the kWh based method can give a better approximation of degradation rates without any hassle. As this method is only dependent on metered inverter data and historic irradiance data (NREL-NSRDB) for selecting less variant months, this method can be used for a quick estimation and overview of the degradation rate and performance of the system.

2.4.5 Application of Performance Index

Performance Index can be used to determine different losses in the system such as temperature loss, soiling loss and so on. Figure 40 shows the monthly % temperature loss and measured output energy for Model G in 2003. This temperature loss was calculated from Temperature Adjustment (TA) in PI calculation where the cell temperature was computed using Sandia's thermal model. It can be seen that approximately 15% of energy was lost in three months, June-August, due to high operating temperatures during the peak summer in Arizona. Figure 41 shows the pie chart of average performance of Model G from 2003-2007. The system loss was assumed to be 15% which includes losses like mismatch, inverter, DC & AC and so on. Also, it can be seen that 12% of annual energy is being lost because of high operating temperatures in AZ and 5% of unknown losses, which may be attributed to soiling, as most of the other losses are already accounted in the computation of Performance Index.

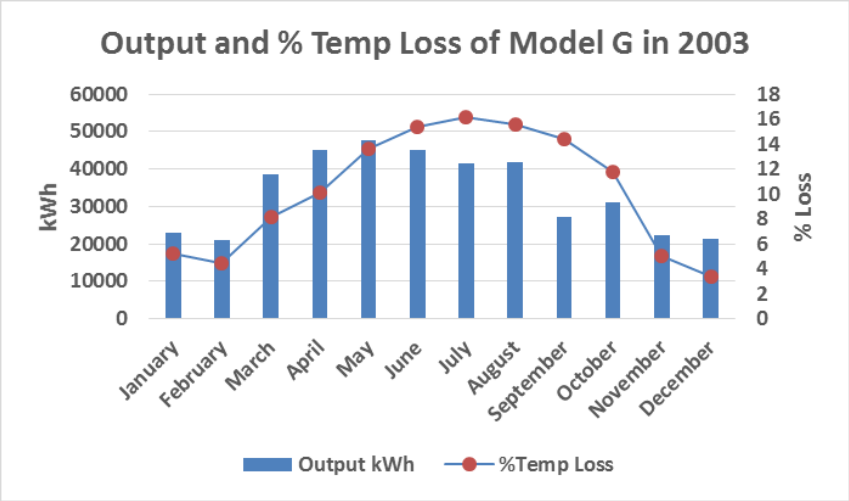

40 Monthly % Temperature Loss and Measured Output Energy for Model G In 2003

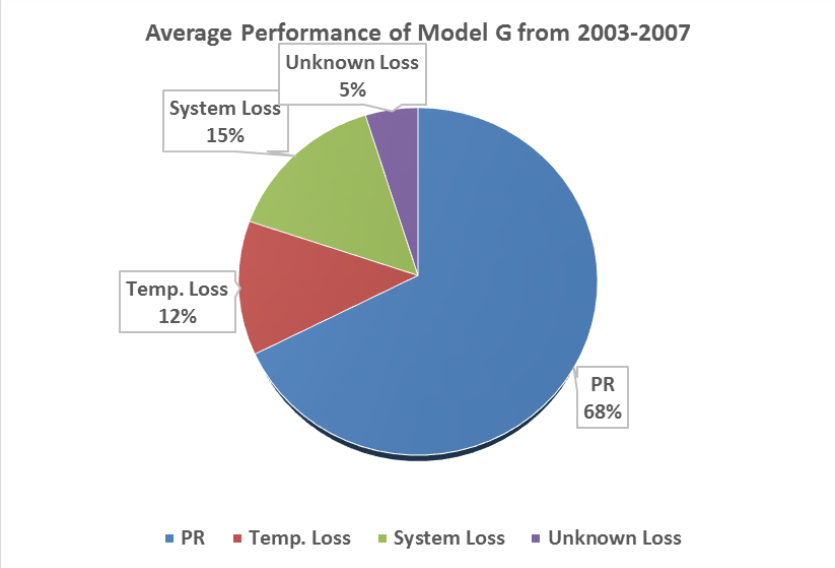

41 Average Performance and Losses of Model G from 2003-2007

As mentioned above, the unknown losses may be attributed to soiling loss and using daily PI, the soiling rate or soil build up rate can be calculated as shown in Figure 42. For this rooftop site at 5 deg. tilt, the soil build rate is calculated to be 0.24%/day which is near the average soiling rate of 0.2%/day for a 5 deg. tilt system reported in the literature [34]. With

no rain events or no cleaning, this build up rate can account for the loss of 24% at the end of the 100th day.

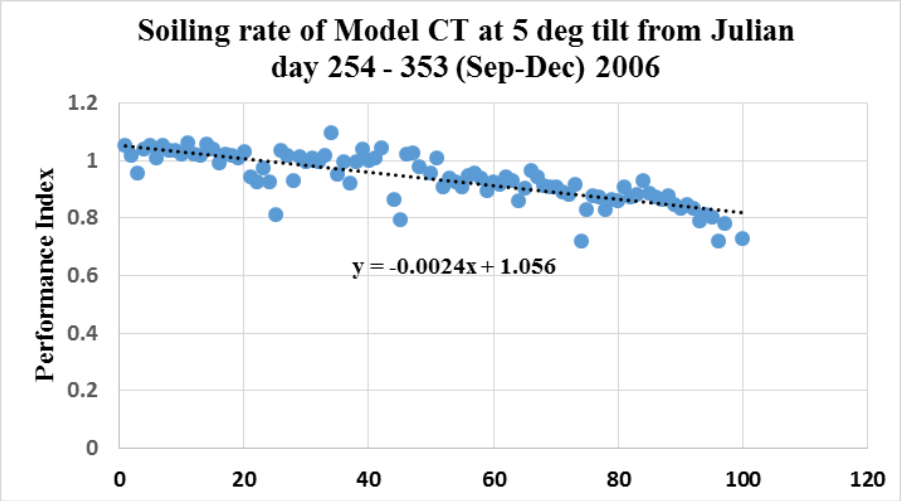

42 Soiling Rate of Model CT from September to December 2006

2.5 CONCLUSION

Degradation rates were calculated using four different methods and were compared with the most accurate I-V measured degradation rate. Degradation rates were calculated from a metered raw kWh method after selecting good months (months with low standard deviation), and had a deviation of ±0.15% from the I-V measured rate (0.9-1.37%/year). This resulted in fairly accurate degradation rates for all three systems than other methods. PR method had a deviation of ±1% in two systems from the I-V measured rate. Though PR method is insolation corrected, the temperature does have a strong effect on rooftop systems, therefore the ratio computed does not give a clear picture of the performance.

PI method resulted in identical degradation rates as the I-V method for Model G and CT, however, the degradation rate for Model HP calculated from the PI method resulted in an unusual positive degradation rate. The meteorology data in this analysis was an important aspect because Model G and CT used a combination of both locally measured data for 5 years and satellite modelled data for 5 years (SolarAnywhere 10X10 km resolution data). On the other hand, Model HP used satellite modelled data only (SolarAnywhere 10X10 km resolution data), which resulted in an erroneous degradation rate for Model HP. In this analysis, there were many uncertainties from the GHI modelling in SolarAnywhere (web based database using SUNY satellite model), POA irradiance modelling in PVSyst using Perez's model, and temperature modelling using Sandia's thermal model. Therefore, for computing a more accurate degradation rate from PR & PI methods, we need to have a well maintained ground mounted meteorology station (to directly monitor POA irradiance and

other weather data and avoid modelling as much as possible) to reduce the uncertainties in the PI analysis. However, meteorology stations are not common to have in all the sites, and depending on satellite weather data for degradation analysis, it may result in a biased degradation rate. This analysis used 10X10 km resolution SolarAnywhere data which resulted in some biased outcomes, but SolarAnywhere also provides an enhanced dataset of 1X1 km resolution which is more accurate, though more expensive, with less uncertainties and can be used to compute better and more accurate results.

In conclusion, the field I-V measurement method is the ideal and best method for degradation rate calculation, followed by PI method, provided POA irradiance and weather data are locally available with a ground mounted station. Metered raw kWh based method, after eliminating bad months with high insolation variability, is ranked third as it is a fairly accurate, simple, fast, and inexpensive technique for degradation rate computation when compared to other methods. PI method, which uses satellite modelled data for irradiance and weather, is placed as fourth whereas, PR method from this study is ranked least as it reflects only the insolation adjusted performance of the system. All the systems investigated in this study appear to indicate that they all degrade linearly. The temperature loss during summer months is above 15%, and approximately 12% over the year for one-axis trackers in Arizona. Soiling loss (build up rate) during the second dry season (mid-September through mid-December) is about 0.24%/day for the rooftop 5^{o} tilted PV modules in Arizona.

REFERENCES

[1] J. Mallineni, B. Knisely, K. Yedidi, S. Tatapudi, J. Kuitche, and G. TamizhMani, "Evaluation of 12-Year-Old PV Power Plant in Hot-Dry Desert Climate: Potential Use of Field Failure Metrics for Financial Risk Calculation," *IEEE Photovoltaic Specialists Conference*, June 2014.

[2] K. Yedidi, J. Mallineni, B. Knisely, S. Tatapudi, J. Kuitche, and G. TamizhMani, "Failure and Degradation Modes and Rates of PV Modules in a Hot-Dry Climate: Results after 16 years of field exposure," *IEEE Photovoltaic Specialists Conference,* June 2014.

[3] G. TamizhMani and J. Kuitche, "Accelerated Lifetime Testing of Photovoltaic Modules" *A report of Solar America Board for Codes and Standards (solarabcs.org)*, 2013.

[4] J. Wohlgemuth, D. W. Cunningham, A. Nguyen, G. Kelly, and D. Amin, "Failure Modes of Crystalline Si Modules", *NREL's PV Module Reliability Workshop, Golden, CO,* February 2010.

[5] M. A. Cluintana, D. L. King, T. J. McMahon, and C. R. Osterwald, "Commonly Observed Degradation in Field-Aged Photovoltaic Modules," *IEEE Photovoltaic Specialists Conference,* May 2002.

[6] D. DeGraaff, R. Lacerda, and Z. Campeau, "Degradation Mechanisms in Si Module Technologies Observed in the Field; Their Analysis and Statistics", *NREL's Photovoltaic Module Reliability Workshop*, Golden, CO, February 2011.

[7] J. Wohlgemuth, "Module Safety Issues", *NREL's PV Module Reliability Workshop*, February 2012.

[8] G. H. Atmaram, G. G. Ventre, C. W. Maytrott, J. P. Dunlop, and R. Swamy, "Long-term Performance and Reliability of Crystalline Silicon PV Modules" *IEEE Photovoltaic Specialists Conference,* May 1996.

[9] L. N. Dumas and A. Shumka, "Photovoltaic Module Reliability Improvement through Application Testing and Failure Analysis," *IEEE Transactions on Reliability,* Vol. R-31, NO. 3, AUGUST 1982.

[10] N. G. Dhere, "Reliability of PV Modules and Balance-of-System Components" *IEEE Photovoltaic Specialists Conference*, January 2005.

[11] Z. Zhang, J. Wohlgemuth, and S. Kurtz, "The thermal reliability study of bypass diodes in photovoltaic modules", *Photovoltaic Module Reliability Workshop*, Golden, Colorado, February 2013.

[12] M. A. Quintana, D. L. King, F. M. Hosking, J. A. Kratochvil, R. W. Johnson, B. R. Hansen, N. G. Dhere, and M. B. Pandit, "Diagnostic Analysis of Silicon Photovoltaic Modules after 20-year Field Exposure," *IEEE Photovoltaic Specialists Conference*, September 2000.

[13] A. Birolini, "Quality and Reliability of Technical Systems: Theory-Practice-Management" Springer-Verlag, ISBN 3-540-40287-X, 2004.

[14] M. Lazzaroni, L. Cristaldi, L. Peretto, P. Rinaldi, and M. Catelani "Reliability Engineering: Basic Concepts and Applications in ICT," ISBN 978-3-642-20982-6, Springer; 2012.

[15] IEC 60812 (2nd edition), "Analysis techniques for system reliability – Procedure for failure mode and effects analysis (FMEA)," 2006.

[16] J. B. Bowles, "An Assessment of RPN Prioritization in a Failure Modes Effects and Criticality Analysis", *Reliability and Maintainability Symposium*, Page 380 – 386, 2003.

[17] D. L. Meier, E. A. Good, R. A. Garcia, B. L. Bingham, S. Yamanaka, V. Chandrasekaran, and C. Bucher, "Determining components of series resistance from measurements on a finished cell", *IEEE Photovoltaic Energy Conversion*, May 2006.

[18] A. P. Dobos, "An improved coefficient calculator for the California energy commission 6 parameter photovoltaic module model", *Journal of Solar Energy Engineering*, vol. 134(2), 021011, March 2012, DOI:10.1115/1.4005759.

[19] D. Jordan and S. Kurtz, "Photovoltaic Degradation Rates - An Analytical Review," *Progress in Photovoltaics: Research and Applications*, vol. 21, pages 12–29, January 2013.

[20] J. Kuitche, R. Pan & G. TamizhMani, "Investigation of Dominant failure mode for Field-aged c-Si PV modules under desert climatic conditions", *IEEE Journal of Photovoltaics*, vol. 4, pages 814–826, May 2014.

[21] Steve Pulver, Daniel Cormode, Alex Cronin, Dirk Jordan, Sarah Kurtz, & Ryan Smith, "Measuring Degradation Rates without Irradiance Data" , University of Arizona, Tucson, & NREL, Boulder, Colorado.

[22] J. Belmont, K. Olakonu, J. Kuitche and G. TamizhMani, "Degradation Rate Evaluation of 26-Year-Old 200 kW Power Plant in a Hot-Dry Desert Climate", IEEE PVSC 2014.

[23] IEC 61724 First edition, "Photovoltaic system performance monitoring –Guidelines for measurement, data exchange and analysis", 1998-04.

[24] http://pvpmc.org/ you need to give more details

[25] D.L. King, W.E. Boyson, J.A. Kratochvill, "Photovoltaic Array Performance Model", Sandia National Laboratories

[26] G. TamizhMani, L. Ji, Y. Tang, L. Petacci and C. Osterwald, "Photovoltaic Module Thermal/Wind Performance: Long -Term Monitoring and Model Development for Energy Rating" NCPV and Solar Program Review Meeting 2003 NREL/CD-520-33586 Page 936

[27] Jaewon Oh, "Building Applied and Back Insulated Photovoltaic Modules:Thermal Models", Masters' Degree Thesis Report, Arizona State University (2010)

[28] https://www.solaranywhere.com/Public/About.aspx

[29] R. Perez, P. Ineichen, K. Moore, M. Kmiecik, C. Chain, R. George and F. Vignola, "A new operational model for satellite-derived irradiances: description and validation", Solar Energy, vol. 73, No. 5, pp. 307–317, 2002

[30] R. Perez,, P. Ineichen,, R. Seals, J. Michalsky, and R. Stewart, "Modeling daylight availability and irradiance components from direct and global irradiance", Solar Energy, 44 (5), 271–289, 1990

[31] T. Townsend, C. Whitaker, B. Farmer, and H. Wenger. "A new performance index for PV system analysis", CH3365-4/94/0000-1036 IEEE First WCPEC, 1994

[32] http://rredc.nrel.gov/solar/old_data/nsrdb/1991-2010/ need more details

[33] http://rredc.nrel.gov/solar/calculators/pvwatts/version1/ need more details

[34] F. A. Mejia and J. Kleissl, "Soiling losses for solar photovoltaic systems in California", Solar Energy, 95 (2013) 357–363.